AIAA SciTech Forum
11–15 & 19–21 January 2021, VIRTUAL EVENT
AIAA Scitech 2021 Forum

10.2514/6.2021-1347



# Exploratory Investigation of Combustion and NVH Emissions Signature of a Drone Jet Engine Fueled with IPK

Valentin Soloiu[1] and Camille Phillips[2]
*Georgia Southern University, Statesboro, GA, 30458, USA*

Cesar Carapia[3] and Aliyah Knowles[4]
*Georgia Southern University, Statesboro, GA, 30458, USA*

Drake Grall[5] and Richard Smith[6]
*Georgia Southern University, Statesboro, GA, 30458, USA*



## Abstract

The pollution from aerospace transportation is rapidly becoming the largest source of greenhouse gas (GHG) emissions. The FAA expects aviation emissions to almost triple by 2050, making the aerospace industry responsible for the release of approximately 25% of the global carbon dioxide budget. These aviation emissions, including $CO_2$ and $NO_x$, as well as other GHGs, contribute to the destruction of ozone layer. Carbon dioxide emissions have a particularly negative effect on humans, leading to airway diseases especially in children and elderly. To combat the addition of further GHG emissions into the atmosphere, it is necessary to increase engine efficiency while reducing the NVH signature. Synthetic kerosene has a high potential for both commercial and military use due to their low soot emissions and their favorable balance of fuel properties. The purpose of this study is to investigate combustion, emissions and NVH produced by combustion of synthetic kerosene (IPK) in a drone single stage gas turbine. Electronic data acquisition systems, including microphones, accelerometers, load cells, Mie scattering for sprays characterization, a constant volume combustion chamber (CVCC) and a state of art FTIR emissions analyzer were employed to during this project on the IPK and the jet engine.

## Nomenclature

| | |
|---|---|
| *ASTM* | American Society for Testing and Materials |
| *CPB* | Constant Percentage Bandwidth |
| *FAA* | Federal Aviation Administration |
| *FFT* | Fast Fourier Transform |
| *FTIR* | Fourier Transform Infrared Spectroscopy |
| *F-T* | Fisher-Tropsch process |
| *IPK* | Iso-Parrafinic Kerosene |
| *ppmV* | Parts per Million by Volume |

---

[1] Prof. Dr. Mechanical Engineering.
[2] Undergraduate student, Mechanical Engineering.
[3] Master student, Mechanical Engineering.
[4] Master student, Mechanical Engineering.
[5] Master student, Mechanical Engineering.
[6] Undergraduate student, Mechanical Engineering.

**Table of Contents**

## List of Figures

# I. Introduction

Greenhouse gases are produced primarily through the burning of fossil fuels for electricity, heat, agricultural processes manufacturing processes, and transportation. Climactic effects from greenhouse gases are expanding and include increased temperatures at the Earth's surface, troposphere, and oceans worldwide, a decrease in snow and ice over the poles due to melting, and growing season lengths (J.I. Hileman 2017). The United States Environmental Protection Agency attribute changes in weather patterns and extreme weather events, rising seas levels, and higher acidity levels in oceans to climate change as well (EPA 2016).

In 2012, transportation emissions accounted for 28% of the total U.S. carbon dioxide emissions, with the aviation industry in particular being responsible for 12% of transportation emissions (3.36% of the total carbon dioxide emissions). The Federal Aviation Administration forecasts that fuel consumption of U.S.-based airlines will increase an average of 1.6 percent per year before 2025 (Romera 2018). Due to this expected increase in fuel consumption, the aircraft industry is looking for ways to improve fuel efficiencies and mitigate greenhouse gas emissions.

The fossil fuel emissions from aviation include carbon dioxide ($CO_2$), methane ($CH_4$), nitrous oxide ($NOx$), and black carbon (soot). Since the bulk of aircraft emissions are produced at cruising altitudes, they have a greater negative effect than greenhouse gases released at the Earth's surface. Figure 1 below displays how at cruising altitude, carbon dioxide, nitrogen oxides, water vapor, sulphates, and soot are released from jet engines. For every gallon of jet fuel burned, approximately 21 pounds of carbon dioxide are emitted (Fleming 2009).

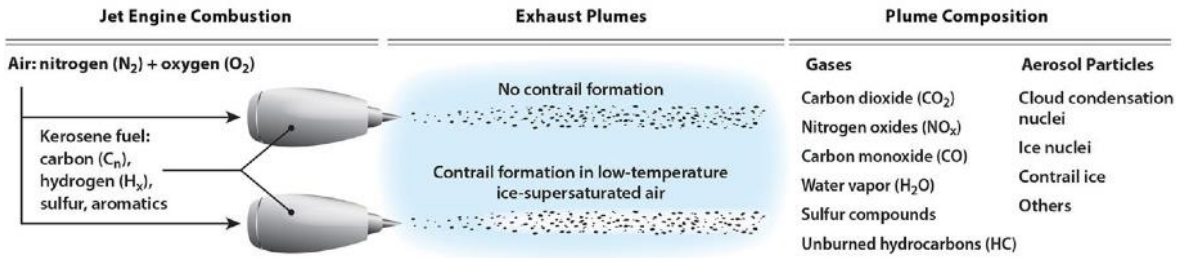


**Figure 1. Emissions from Aircraft at Cruising Altitude (Stein 2020)**

As air transport is the leading sector in demand for oil, 31% of oil in the U.S. goes to the creation of distillates for diesel fuel, jet fuel, and fuel oils and 46% of oil by volume is used in the production of gasoline. While the global aviation industry consumes around 5 million barrels of oil per day, in 2010, the US consumed 27% of the worldwide demand of jet fuel (C. Zhang 2016). The global demand for jet fuel is expected to grow at a mean growth rate of 1.9% per year until 2025, even with the limited fossil fuel reserve putting limitations on fuel production (Romera 2018). With energy always in demand, petroleum prices continue to increase with the spikes in consumption, leading the aviation industry to explore economical and environmentally friendly options for jet fuel production.

As air traffic continues to increase, noise caused by aircraft operations in the surrounding areas of airports is becoming a more prevalent issue, both environmentally and technologically, in today's society (Mofid Gorji-Bandpy 2012). Many of the health problems attributed to aviation related noise stem from sleep disruption or deprivation. The FAA strives to control aircraft noise through measures such as noise reduction at the source (development and adoption of quieter aircraft), soundproofing and buyouts of buildings near airports, operational flight control measures, and land use planning strategies (Swift 2010). In an effort to reduce noise at the source, this study analyzes the noise and vibrations produced when synthetic fuel is burned within a single stage experimental turbojet engine.

The standard jet fuels used in the United States are Jet A for civil aviation and JP-8 for military. Possible alternatives to these standard fuels are synthetic fuels derived from coal and natural gas using the Fischer-Tropsch process. This method converts raw carbon sources such as coal, natural gas, biomass, or organic waste into synthesis gas before indirectly liquefying them into hydrocarbons and refining them into fuels (Zhou, Liu and Wang 2015). Some Fischer-Tropsch fuels are certified for commercial use as blends with standard fuels and more fuels are under development using this method. In this study, the fuel properties as well as the combustion, gaseous emissions, noise, and vibrations characteristics of iso-paraffinic kerosene, a Fischer-Tropsch synthetic fuel, and Jet A, as the standard jet fuel, are examined and compared. Additionally, an in-depth analysis noise vibrations and harshness of IPK combustion within a single stage turbo-jet engine at different speeds will be performed.

# II. Literature Review

***Fuel Properties***

The Fischer-Tropsch process is an indirect synthesis that provides liquid hydrocarbon fuels as an alternative to direct coal gasification. This technology converts raw carbon sources such as coal, natural gas, biomass, or organic waste into synthesis gas before indirectly liquefying them into hydrocarbons and refining them into fuels (Tara J Fortin 2015). The process includes gasification of the input carbon source to form a synthesis gas composed of carbon monoxide and hydrogen. Conversion of the syngas into primary products of wax, hydrocarbon condensate, tail gas, and reaction water occur before the wax is chemically split into hydrocarbon liquids parts that smaller by molecular weight. The extra hydrogen from the tail gas and feed syngas stream are extracted using a recovery unit. Reaction products are portioned into diesel and jet fuel.

Classification of Fischer-Tropsch fuels is based on the source of the synthesis gas; when a liquid fuel is synthesized from coal, it is called a coal-to-liquid (CTL). In the same way, a gas-to-liquid (GTL) is when a liquid fuel is synthesized from gas. The compositions of the F-T fuels are dependent upon the crude carbon source from which the fuel was derived in addition to the specific refining process implemented (Tara J Fortin 2015). Some F-T fuels from the hydrotreated renewable jet fuel (HRJ fuel) category are certified for commercial use as blends with the previously mentioned standard jet fuels (Tara J Fortin 2015). There are stringent federal requirements to become a qualified blending agent with the acceptable conventional fuels.

According to Julia Heimberger and Martin Muinos (Julia Heimberger n.d.), there are four molecular classes of aviation fuel composition: paraffins (alkenes), olefins, napthenes, and aromatics. Paraffinic fuels are also known as kerosenes and are refined in the Fischer-Tropsch process from natural gas, biomass, or vegetable oils and animal fats. Olefinic fuel is produced from unsaturated hydrocarbon compounds, called olefinic hydrocarbons, that contain at least one carbon to carbon double bond. Generated from man-made oil and natural gas compounds, olefinic fuel is produced from crude oil refineries and chemical plants. Cycloparaffins or napthenes have the same chemical formula as olefins but are paraffins that are bent into a ring shape (Sadeghbeigi 2012). The high-performance gasoline that is derived from napthenes has a higher aromatic content and is heavier than gasoline. Made from crude oil, aromatics are base components of gasoline. Aromatics can be manipulated into chemical substances in mixtures to increase fuel performance.

**Table 1. ASTM Standards and Properties of Conventional and Alternative Jet Fuels (Chi Zhang, 2014)**

| Property | ASTM Standard | Jet A | Sasol IPK |
|---|---|---|---|
| POSF number | -- | 4658 | 5642 |
| Composition | | | |
| n – Paraffins (wt%) | -- | 28 | 2.1 |
| Iso – Paraffins (wt%) | -- | 29 | 88 |
| Cyclo – Paraffins (wt%) | -- | 20 | 9 |
| Aromatics (wt%) | Report | 20 | <0.5 |
| Total Sulfur (wt%) | Max 0.3 | -- | <0.001 |
| Distillation | | | |
| Initial boiling point (°C) | Report | 158 | 149 |
| 10% recovered (°C) | Max 205 | 184 | 166 |
| 20% recovered (°C) | Report | 192 | 170 |
| 50% recovered (°C) | Report | 213 | 180 |
| 90% recovered (°C) | Report | 248 | 208 |
| Final boiling point (°C) | Max. 300 | 269 | 228 |
| Flash point (°C) | Min. 38 | 47 | 44 |
| Freezing point (°C) | Max. -47 | - 49 | < -78 |
| Density @ 15 °C (kg/m$^3$) | 665-840 | 806 | 762 |
| Viscosity @ -20 °C (cSt) | Max. 8.0 | 5.2 | 3.6 |
| Neat heat of combustion (MJ/kg) | Min. 42.8 | 42.8 | 44 |
| Smoke point (mm) | Min 19.0 | 21 | > 40 |
| H/C molar ratio | -- | 1.957 | 2.119 |
| Property | ASTM Standard | Jet A | Sasol IPK |
| Molecular weight (g/mol) | -- | 142 | 156 |

In reference to Table 1 ASTM Standard and Properties of Conventional and Alternative Jet Fuels (Chi Zhang 2014), by weight percentage, Jet A is composed of more n-paraffins, cyclo paraffins and aromatics. By weight percentage, the F-T fuel is primarily composed of iso-paraffins and leads in sulfur weight percentage against Jet A.

Prominent fuel properties that effect combustion behavior include hydrogen to carbon molar ratio (H/C), molecular weight (MW), derived cetane number (DCN), and threshold sooting index (TSI). Over the past one hundred years, fuel usage has trended towards higher hydrogen to carbon molar ratios because as the hydrogen to carbon ratio increases, energy efficiency increases and $CO_2$ emissions decrease (Balachandar Gopalakrishnan 2019). Recently, lower carbon content has been achieved in natural gas in comparison to oil. Biofuels contain even lower carbon content and other options like hydrogen fuel have a zero carbon to hydrogen ratio. The H/C ratio can be a good indicator of efficiency and emissions characteristics of fuels. In a study concerning the fuel properties during blending of iso-paraffinic kerosene and jet fuel performed by (Richard Striebich 2008), as FT fuel is added to standard jet fuels (creating an FT blended fuel), the blends show increased hydrogen content, thereby improving the H/C ratio.

The molecular weight (MW) of a fuel is defined as the ratio of the average mass of one molecule of a fuel to one twelfth the mass of a carbon-12 atom. (Richard Striebich 2008) found a linear dependence of the fuel flash point on percentage of FT blend. According to the same study by (Richard Striebich 2008), dependence of flash point on percentage of FT fuel was due to the similarity of volatility and molecular weight to that of standard aviation fuels.

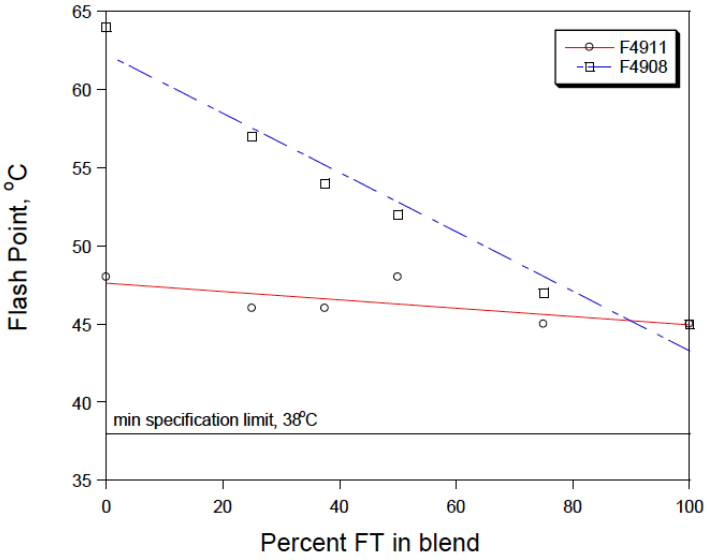


**Figure 2. Dependence of flash point (ASTM D93) on blend percentage of FT-derived fuel (Richard Striebich, 2008)**

A fuel's derived cetane number (DCN) is determined from the ignition delay (ID) and combustion delay (CD) times, as calculated with equation (1) (J. Yanowitz 2017). The ignition delay period is between the time of fuel injection and the time when autoignition occurs. Combustion delay is the time between injection and the peak pressure of combustion. Typically, fuels that have a high derived cetane number have a short ignition delay, meaning that ignition occurs quickly after fuel injection starts. Similarly, longer ignition delays are related to lower cetane numbers. A derived cetane number is based on fuel ignition delay and combustion delay (using a constant volume combustion chamber) and therefore is the measurement that will be used for analysis in this study.

$$DCN = 13.028 + \left(\frac{-5.3378}{ID}\right) + \left(\frac{300.18}{CD}\right) + \left(\frac{-1267.90}{CD^2}\right) + \left(\frac{3415.32}{CD^3}\right) \quad (1)$$

Ignition delay as defined in this study, is the time lag between the start of fuel injection and the start of combustion when the air fuel mixture ignites. An ignition delay that is too short generates a low-quality combustion and reduced efficiency due to insufficient air-fuel mixing (Setiawan, Wahono and Lim 2020). As ignition and combustion delay increases, the premixing of fuel and air also increases which reduces the duration of combustion. Longer ignition and combustion delays allows for a more homogenous air-fuel mixture leading to better quality combustion. When

examining jet fuels and how they combust, ignition and combustion delay is a primary factor in determining the efficiency of the fuels' burn.

(Sylvester Abanteriba 2016) found that ignition delay is dependent on fuel volatility. Similarly, volatility is tied to the composition and structure of the fuel. In combination with findings from (R. 2012), longer ignition delay times from iso-paraffins and aromatics were credited to the higher stability of the molecular structure that needs high activation energies to spark the combustion process. (Ghosh P. 2006) observed that in most cases, fuels with high concentrations of n-paraffins have low ignition delay times. When examining the fuel compositions of Jet A and IPK, from fuel composition analysis between Jet A and IPK, Jet A contains a higher percentage by weight of n-paraffins over IPK. IPK is additionally expected to have a higher ignition delay time than Jet A from its high iso-paraffin content.

A threshold sooting index (TSI) is a ranking system for the sooting tendency of fuels. A combustion cycle can be incomplete due to reduced supplies of oxygen and lower than ideal temperatures. Soot is produced from incomplete combustion, made primarily of black carbon. According to (Yi Yang 2007), TSI allows for the best prediction of soot formation in turbine combustion against other parameters that are often implemented for predictive measurements of soot formation. (Robert J. Santoro 2007) observed that the threshold sooting index for diffusion flames is a sum of a constant *a* times the ratio of molecular weight to smoke point and a second constant *b*. Both constants are dependent on the apparatus for smoke point measurement. According to (Yi Yang 2007), the TSI has a linear correlation with the ratio of fuel MW and smoke point in a diffusion flame. A high smoke point means that a fuel has a low smoke producing tendency. Generally speaking, the more aromatics a fuel contains, the more smoke it produces, meaning that it has a lower smoke point. An ideal combination for a fuel to have a low TSI (producing a low amount of soot) would be a low molecular weight and a very high smoke point. This combination would make the ratio very small, producing a low TSI. According to Figure 2, Jet A has a MW/ smoke point ratio of 21/142 (0.14789) while IPK has a ratio of 40/156 (0.25641). Because Jet A has a lower ratio, it can be assumed that Jet A will have a lower soot production that IPK.

According to (Tara J Fortin 2015), other important properties of jet fuels include thermo-physical properties like viscosity, lower heating value (LHV), density, and thermal stability (TGA/DTA). Closely tied to fuel efficiency, viscosity is the property of internal resistance against flow. High fuel viscosity can cause damage to a fuel pump during cycle process from the resulting high pressure. Additionally, improper fuel injection due to a high fuel viscosity could lead to combustion inefficiency. Low fuel viscosity could cause insufficient lubrication of the injector leading to improper injection of the fuel. Viscosity affects the injection droplet velocity as well as the rate of fuel injection, fuel atomization, and fuel penetration.

The LHV of a fuel is the amount of heat released during combustion. The specific energy output of the combustion of a fuel is determined by the LHV. TGA/ DTA (Thermogravimetric analysis / differential thermal analysis) are evaluations of chemical reactions that provide properties of fuels such as enthalpy, thermal capacity, mass changes, and the coefficient of heat expansion. TGA measures changes in weight of a fuel in relation to changes in temperature of a fuel during combustion. From this analysis, a measured weight loss curve can be acquired. The derivative this curve is useful in understanding the point of most weight loss, allowing for the determination of thermal stability of the fuel. DTA quantifies the heat exchange between the fuel and the surrounding control volume and is able to highlight both endothermic (vaporization of fuel) and exothermic reactions (fuel oxidation).

The fuel properties analyzed in this study were viscosity, LHV, TGA/DTA, cetane number (including NTC, LTHR, and AHRR) and their combustion characteristics that were evaluated using a constant volume combustion chamber (CVCC).

***Gaseous Emissions***

The chemical composition of Jet A and IPK fuel can have a large impact how the fuel combusts. Additionally, the quantity and type of emissions released from fuel burn is dependent on how the fuel combusts. Emissions from jet fuel combustion processes include carbon dioxide, water vapor, nitrous oxides, hydrocarbons, volatile organic compounds, carbon monoxide, sulfur oxides, and particulates (Aviation & Emissions A Primer 2005). Jet fuel exhaust is made up of 10% carbon dioxide. When fuel combines with oxygen in the air during a complete combustion cycle, carbon dioxide is released and mixes with atmospheric gases. These mixtures of carbon dioxide have a direct warming effect on the earth and their long-life cycles cause them to be especially detrimental to the environment. Jet exhaust is 10% water vapor, as it is released into the atmosphere when the hydrogen in the fuel mixes with oxygen in the air. Contrails form when water vapor freezes in the high-altitudes, later causing clouds which trap infrared rays. Although

they do not have long life spans, the trapped infrared rays have a warming effect that is greater than the effect of all carbon dioxide emissions combined.

Hydrocarbons and carbon monoxide particulates are created when jet fuel does not completely combust. Particulates are atmospheric aerosol particles that are microscopic in size. Particulate matter can be solid or liquid and their microscopic size allows them to be suspended in the air for extended periods of time (Mohamad P. Zakaria 2018). Ultra-fine particles (UFPS) and polycyclic aromatic hydrocarbons (PAHs) are $1/1000^{th}$ the width of a human hair and linger in the air for up to two weeks. They have the ability to permeate filtration and conditioning units in buildings and cars and they sustain their shape over long distances of travel. They also have the capacity to breach soft body tissues and enter bloodstreams (Mohamad P. Zakaria 2018).

Hydrocarbons (HC) are hazardous air pollutants and are often called volatile organic compounds (VOCs). Incomplete combustion causes carbon monoxide and hydrocarbon particulates to form that generate contrails and later cirrus clouds which negatively affect the environment. Additionally, the carbon monoxide emissions produced from incomplete combustion are particularly harmful to humans. In this study, carbon monoxide (CO), carbon dioxide ($CO_2$), water vapor ($H_2O$), methane ($CH_4$), sulfur dioxide ($SO_{2)}$, nitrous oxides ($NO_x$), and total hydrocarbon (THC) emissions will be analyzed in this study.

***Noise Vibrations and Harshness***

Combustion noise in gas turbines has been found to occur in the 200 – 600 Hz frequency range, at which point the flame created by the reaction produces sounds power, the size of which depends on the geometry of the gas turbine (Dowling and Mahmoudi 2014). This chemical flame reaction causes high levels of sound to emanate from the turbine, Therefore, it can be assumed that there is a direct relationship between the sound output and the reaction rate time derivative all averaged on the combustion volume. The state of the combustion flame must also be considered. When the flame is turbulent, the combustion region is larger, and the reaction has little directionality (Lefebvre and Ballal 2010). The rate of fuel reaction during combustion as well as the vaporization rate of the fuel could also be of importance to the understanding of acoustic combustion effects. Figure 3 below displays the main sources of jet noise (Dowling and Mahmoudi 2014).

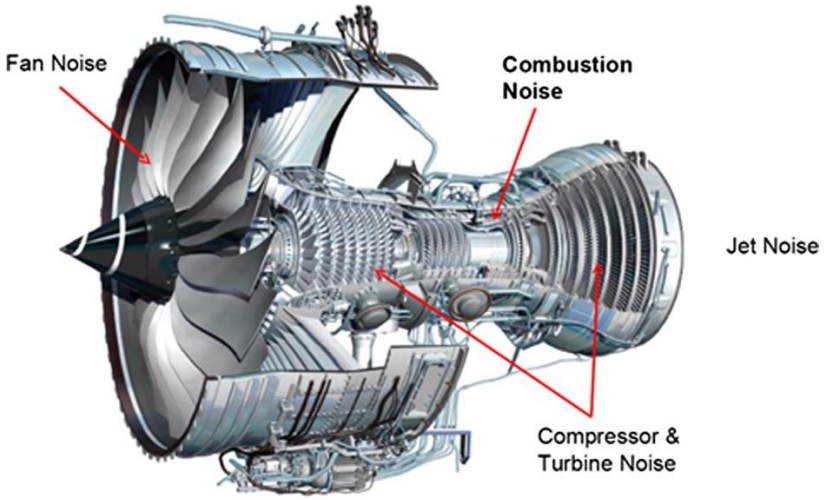


**Figure 3. Main Sources of Jet Noise (Dowling and Mahmoudi 2014)**

The sound pressure levels between 0-1500 Hz increase with burner power level and primary flow rate (Kiameh 2002). The turbulent mixing of unburned fuel and air with the hot combustion products has a near resonance below a critical frequency of 500 Hz, which means that the conversion from thermal energy to acoustic energy of the turbulent flame is of great importance. Large scale fluctuations in turbulence from open premixed flames within the turbine cause fluctuating heat release, leading to downstream velocity fluctuations. High levels of noise generation could be caused by these velocity fluctuations.

Noise from combustion occurs in a confined geometry in two ways: directly and indirectly. Direct sound generation is caused by the rate of heat release and combustion, which is amplified by the boundaries of the combustor geometry (Dowling and Mahmoudi 2014). Meanwhile, indirect sound generation is due to the convection of hot spots throughout the nozzle region and can be considered a major source of noise in the combustor. Indirect noise sources can also be found within the entropy hot spots in regions of accelerated mean flow.

The majority of turbine sound comes from the inlet, exhaust, and casing. The powerful mixing of the turbulent exhaust gases and atmosphere cause the jet exhaust noise. The highest frequency noise emanates from the small eddies nearest to the outlet exhaust, with the turbulence of the larger eddies causing lower frequencies further downstream (Noise Control Suppression 2018). Because of the large number of rotating blades in a turbine compressor, the compressor section of a turbine has the highest sound level pitch. The frequency, in Hz, of the blades can be found by the number of blades multiplied by the RPM speed. Figure 4 describes the contribution areas of the turbine to the total engine noise perceived (Dowling and Mahmoudi 2014).

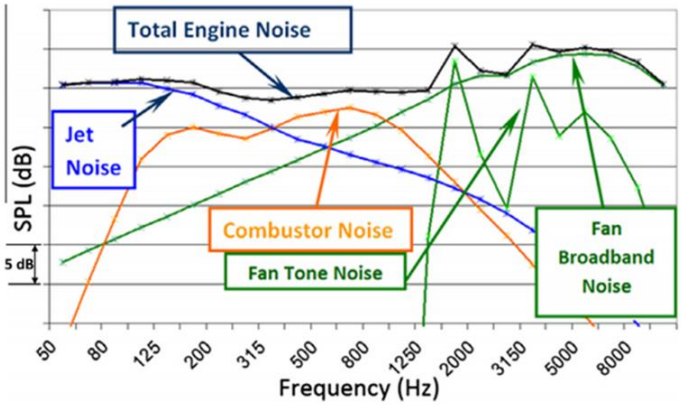


**Figure 4. Combustion noise sources in a gas turbine (Dowling and Mahmoudi 2014)**

There are various sources of noise in the turbine engine. Sound generation from the fan region can be considered either broadband or tonal. Broadband noise is typically random and generated by the rotor whereas tonal noise can correlate to the RPM of the engine as well as the shaft order, as the rotor wakes impinge on stator vanes (M. Gorji-Bandpy 2012). It was also found that the combustion and jet noise decrease as the exit velocity increases.

Every aircraft experiences a unique set of normal vibrational patterns during operation due to mass distribution and structural stiffness at certain frequencies. Aircraft noise is generated from various sections within an aircraft engine, to include the air frame, compressor, turbine, combustor, and jet exhaust (N. A. O. Engineering 2010). A large amount of noise comes from the air frame during take-off and landing, due to the turbulent, separated flow around different parts of the landing gear (AJ 2017). Air frame noise is also produced from air flowing over and around the aircraft during flight, and when turbulent flow occurs along the wing slats when the landing gear is deployed. The leading-edge slat and trailing edge slat regions have been found to be the sources of high tonal noise, or noises that occur at a single frequency, and this tonal noise significantly increases the perceived noise level (AJ 2017). In reference to noise produced from the turbine, the majority of the noise comes from the fan sections.

***CFD Simulation***

(Gicquel, Staffelbach and Poinsot 2012) conducted an extensive study dedicated to improving the use of LES methods for combustion simulation in real gas turbine engine designs. (Gicquel, Staffelbach and Poinsot 2012) comments on the viability of LES as an alternative to the other two extreme numerical tools RANS and Direct Numerical Simulation (DNS). While both RANS and DNS methods provide accurate and concise data, the time and resources required to attain results is daunting and can be inaccessible for a variety of applications. While LES requirements can be as high if not more intensive than RANS or DNS methods in recent years LES and RANs have become more viable options.

(Fooladgar, Toth and Duwig 2019) performed a study dedicated to developing a numerical flameless combustion model for the post processing of a gas turbine combustor model. LES utilizing Finite Rate Chemistry

(FRC) combustion modeling was incorporated along and with an extensive chemical library. The combustor model geometry was developed based off of a previous design given in the literature. The model was incorporated specific boundary conditions and then simulated multiple times for the purpose of validating the flameless model. Finally, a post processing tool was implemented to compare the large volume of data produced from simulation. It was revealed that stratified mixing produces much larger reactive zones compared to the premixed applications. This resulted in the elimination of thine flame fronts due to the large volume of homogenous heat being released in these larger zones.

(Zettervall, et al. 2019) Performed a combination of experimental and computational methods on a modified annular style gas turbine combustor utilizing both methane ($CH_4$) and ethylene ($C_2H_4$) fuels. The main focus of the study was to examine the combustion instabilities present during operation of the gas turbine engine. Experimental testing showed that $CH_4$ and $C_2H_4$ behaved differently than originally expected. $CH_4$ had much larger flames than $C_2H_4$ which affected interactions between flames. The computational simulation utilized an FRC LES method and was used to compare the results of the experimental. The simulation validated the experimental results showing agreements in frequency and heat release.

(Tyliszczak, Boguslawski and Nowak 2016) conducted a numerical study on the combustion process in a gas turbine engine with single and multi-point fuel injection systems to decrease emissions. The study utilized the RANS approach with k-ε model and the LES with Wall Adapting Local Eddy Viscosity (WALE) subgrid model. The simulation featured a steady flamelet model that allowed for multiple species and reactions to be model along with NO chemistry availability. The simulation for single point fuel injection validated the numerical results. The multi-point fuel injection revealed that the distribution of reactants and corresponding boundary conditions can have significant impact on the overall composition present in the chamber. However, even with this change in composition very little change occurs in the resulting emissions production. Meaning that the reduction in emissions was a failure.

(Shakeel, Sanusi and Mokheimer 2017) conducted a computational analysis in which combustion was modelled in gas turbine combustor using methane oxy-fuel blend. The modelling tested radiation modelling and combustion chemistry utilizing a combination of Westbrook-Dryer equations, Jones-Lindstedt equations, and weighted sum of gray gas radiation models (WSGGM). The results showed that the Westbrook-Dryer equations were unable to model the flame development at all. The Jones-Lindstedt and WSGGM method were able to measure the flame development, but not to a desirable accuracy. This method may offer significant advantages with further research; however, it is not reliable enough to warrant usage for this experiment.

(Ryder, et al. 2010) performed a computational fluid dynamic (CFD) simulation to develop and theoretically test combustor designs that could handle a wider range of fuel blends. The reasoning behind this was to increase performance and fuel efficiency of both civil and military grade jet engines. A base line using S8 and Jet A fuels was performed on a trapped vortex combustor (TVC) using CFD software. An adjusted combustor model was then developed, and a base line test was performed using fuel blends such as JP-8 at 0% S8, at 50% S8 and 50% JP-8, and at 100% S8. The results showed that the adjusted combustor geometry had similar performance, and that some consideration can be made for updated combustor geometries and fueling schemes.

(Wawrzak, et al. 2019) performed a study to analyzed annular style combustor geometries. The main goal was to analyze the existence of global instabilities during the combustion process and observe the effects on the flow. The experiment was done by numerically analyzing the model using LES methods where the Reynolds number, Re, and inner shear layer thicknesses are adjusted over nine separate trials. The results showed that two spirals formed in the flow field at the central recirculation zone (CRZ) and then further downstream in outer section of the designated mixing region resulting in asymmetrical flow. This was due to instabilities present just before the CRZ and due to the various flow velocities circulating in these zones. While this evidence seemed promising, no definitive conclusion could be drawn as to the exact instabilities.

(Rotaru 2017) conducted a numerical study observing combustion chamber field flow using CFD to analyze combustion chamber geometry. Increasing the possibility for air and fuel mixture circulation in the primary zone of combustion allows for greater performance is a main concern. Allowing higher turbulence formation and optimal temperature radiation distribution are key in increasing overall performance in gas turbine engines. The study concluded that the distribution of holes within the combustion chamber liner does not need to be symmetric, meaning that these holes are positioned to increase the amount of turbulence.

## III. Thermo-physical properties of IPK and Jet A

***Fuel Characterization***

The thermo-physical properties of IPK and Jet A were examined to include viscosity, lower heating value (LHV), thermogravimetric and differential thermal analysis, ignition delay, combustion delay, and derived cetane number. The combustion properties were obtained using a constant volume combustion chamber (CVCC), while the other values were attained through a variety of techniques. IPK and Jet A were tested separately as non-blended samples where the specific net fuel qualities could be analyzed. The fuel properties that were determined are shown in Table 2.

**Table 2. Fuel Properties Comparison for IPK and Jet A**

| Properties | IPK | Jet A |
|---|---|---|
| **Density (g/cm$^3$) @ 15** °C | 0.762 | 0.806 |
| **Lower Heating Value (MJ/kg)** | 40.74 | 41.51 |
| **Dynamic Viscosity (cP) @ 40** °C | 0.995 | 1.320 |
| **Ignition Delay (ms)** | 5.31 | 3.26 |
| **Combustion Delay (ms)** | 17.17 | 5.01 |
| **Derived Cetane Number** | 25.88 | 47.96 |

*Properties determined using on site equipment.
Batch # 11POSF7629 for the synthetic kerosene and Batch # 13P0SF10325 for Jet A.

***Dynamic Viscosity Determination***

A Brookfield DV II Pro rotational viscometer was used to measure the fuels' dynamic viscosity. Viscosity recordings of the fuels took place with increasing temperature increments of 2°C from 26°C to 90°C, the spindle speed was maintained constant at 200 rpm. The fuels' viscosity was found to dependent on temperature. The dynamic viscosity influences the spray penetration from the fuel injector into the combustion chamber, fuel atomization quality, and droplet velocity during injection. It was observed that the viscosity, in cP, of IPK was 25% lower of the viscosity of Jet A when measured at 40°C as seen in Figure 5 suggesting a better atomization in IPK sprays.

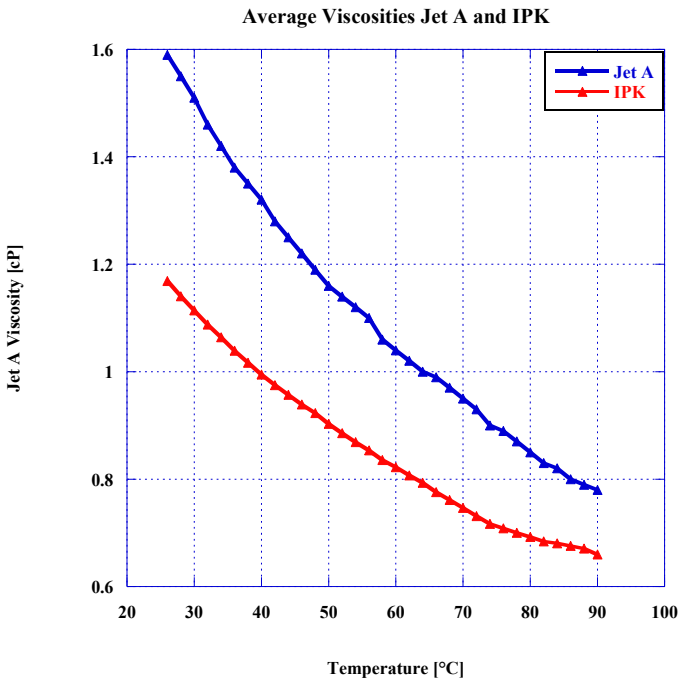


**Figure 5. Dynamic Viscosity of Jet A and IPK**

***Lower Heating Value Determination***

A Parr 1341 constant volume calorimeter was used to measure the fuels' lower heating value (LHV). The LHV of Jet A obtained in the apparatus had an average value of 41.51 MJ/kg, compared to the LHV of IPK, which was measured at 40.7 MJ/kg.

***Low Temperature Heat Release Analysis by Thermogravimetric/Differential Thermal Analysis***

A Shimadzu DTG-60 was utilized to conduct thermogravimetric (TGA) and differential thermal (DTA) anlaysis of Jet-A and IPK for its vaporization rate and energy realease charecteristics. A controlled environment was maintained by constantly purging the system with low moisture compressed air at an airflow rate of 15 mL/min and an incremental temperature rise rate of 20°C/min, with a starting temperature of 20°C and a peak temperature of 600°C. The TGA rate of vaporization per mass % of each of the fuels and the DTA measured the endothermic/exothermic energy levels for both fuels tested against a inert baseline of alumina power. Alumina power looses little to no mass when subjected to high temperatures..

The results for the TGA analysis can be found in Table 3 and Figure 6. It was observed that IPK was more volatile than Jet-A as 10% of its mass (TA10) was vaporized at 70.5°C compared to Jet A's 10% mass vaporization occuring at 83.0°C. The lower temperature TA10 suggests a fast vaporisation of droplets in spray and earlier mixture formation for IPK, potentially offseting the lower DCN of IPK and shortening the ignition delay. As the temperature rises further, the vaporization rate of IPK rises further than Jet-A. IPK reaches a TA90 at 132.2°C in comparison to Jet-A at 164°C. The higher volitility of IPK is advantageous for combustion as it allows for a greater mixing with the air for a more homogenouss air/fuel mixture during combustion.

**Table 3. TGA results Jet A and IPK**

| | Jet-A | IPK |
|---|---|---|
| **TA10** | 83.0 °C | 70.5°C |
| **TA50** | 130.12°C | 108.21°C |
| **TA90** | 164°C | 132.2°C |

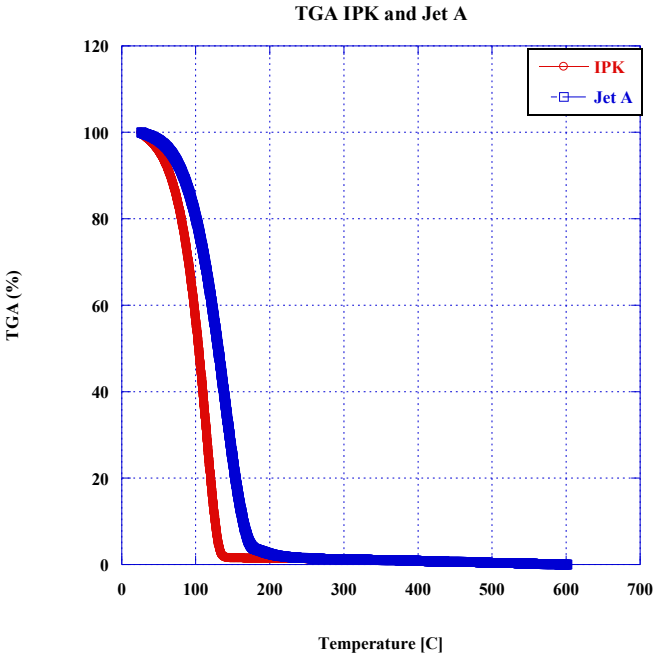


**Figure 6. TGA analysis of IPK and Jet A**

The DTA analysis of Jet A and IPK was performed to observe the low temperature heat release characteristics of the two fuels during combustion. The results of this analysis are shown in Figure 7 below with units in microvolts per milligram. The endothermic reaction of each fuel is exposed in the cocave negative segments of each curve in which energy is absorbed, while the exothermic reaction is displayed in the concave positive portions of each curve as energy is released. It was found that IPK has a greater endothermic reaction than Jet-A, as the minimum of the IPK curve was lower than that of the Jet A curve. IPK reached a minimum value of 124.6°C with the minimum value for Jet-A occuring at 152.4°C. IPK then exhibited a greater exothermic reaction with a peak at 160°C, while the Jet A had a slower heat absorption from room temperature to 200°C where it released the energy.

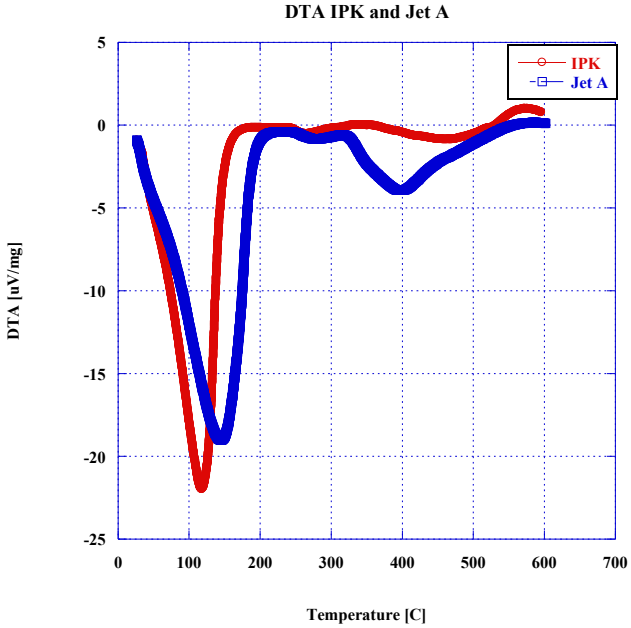


**Figure 7. DTA analysis of IPK and Jet A**

***Spray Analysis with MIE Scattering He-Ne Laser***

A Malvern Spraytec He-Ne laser was utilized to measure the atomization properties of Jet-A and IPK utilizing Mie scattering and Fraunhofer diffraction theories. The experimental apparatus shown in Figure 8, consists of a Malvern He-Ne laser optical system. Fuel injection was done 100mm from the path of the laser using a single hole pintle type witness injector. Using the system shown in Figure 8, data was recorded at a rate of 10kHz at atmospheric temperature and with an injection pressure of 180 bar. Sampling was taken 0.1 ms after the injection initiation and lasted for 5 ms.

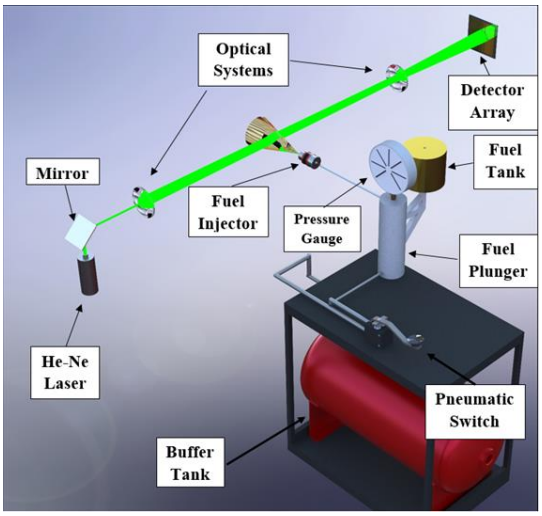


**Figure 8. MIE Scattering Malvern Laser Experimental Configuration (Soloiu, Wiley, et al. 2020)**

Data was collected on the Sauter Mean Diameter (SMD) and the volume frequency distribution for both neat Jet-A and IPK. This data was then displayed as a function of time in Figure 9. From the collected data, IPK has both a smaller SMD and a larger spray volume distribution. A smaller SMD for IPK is more favorable for rapid vaporization and early mixture formation and it is confirmed by the lower viscosity and density of IPK obtained in the experiments presented above. The peak in the volume spray distribution is an indication of the most prevalent droplet size at the given time.

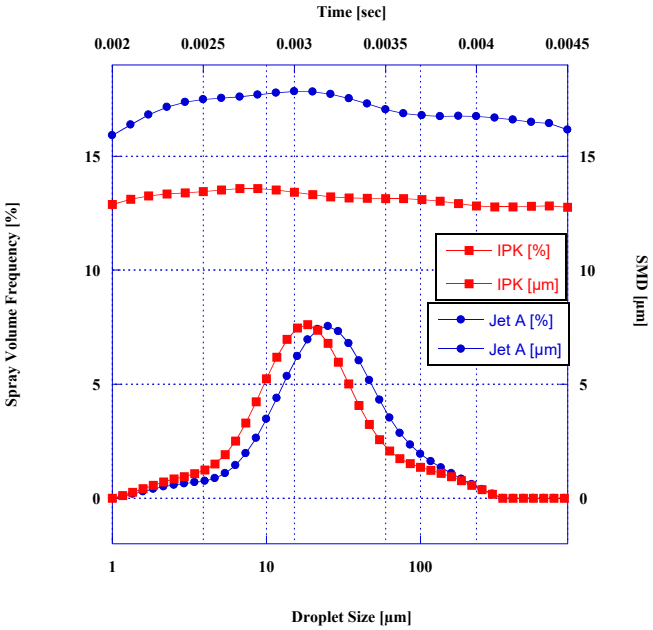


**Figure 9. Spray Droplet Distribution of Jet A and IPK**

***Combustion Experimental Procedure***

A PAC 510 constant volume combustion chamber (CVCC) shown in Figure 10, was utilized under ASTM standard D7668-14a testing parameters for the measurement of the combustion properties of neat IPK and Jet-A. The CVCC uses an electrically controlled common rail system to inject precise amounts of fuel for each combustion cycle. The CVCC also consists of a 6-orifice piezoelectric injector (1), a uniform heated combustion chamber (2), a combustion pressure sensor (3), and injection pressure sensor (4) as seen in the full model in Figure 10. The cross-section model in figure 10 depicts the test injector (1) and the spray distribution (2) in the combustion chamber.

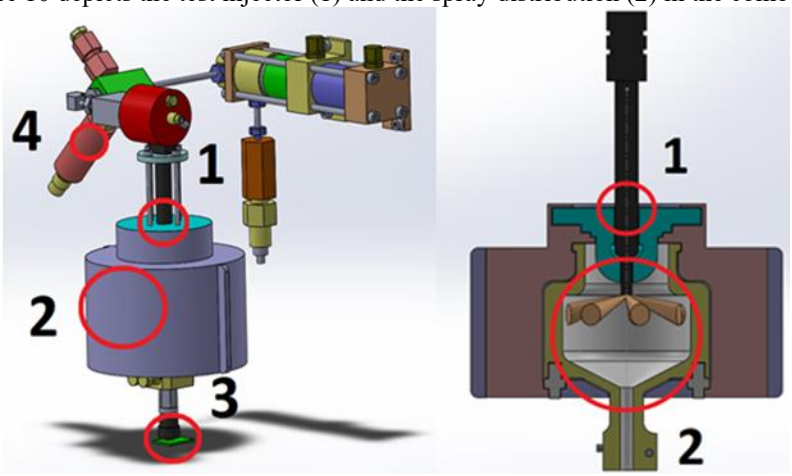


**Figure 10. CVCC model (Soloiu, Wiley, et al. 2020)**

The parameters outlined in ASTM standard D7668-14a are shown in Table 4 and include combustion chamber wall temperature, chamber pressure, injection pulse width, injection pressure, and coolant temperature. These parameters where held for all 15 combustion events per each test fuel with combustion pressure recorded for each event. The 15 combustion events pressure data was utilized in Equation (1) to determine the fuels derived cetane number (DCN) with the use of ignition delay (ID) and combustion delay (CD). DCN is computed via the PAC CID 510 onboard computer.

**Table 4. ASTM D7668-14.a Standard Testing Parameters in a CVCC**

| **ASTM Reference parameters:** | |
|---|---|
| **Combustion chamber Wall Temp.** | 595.5℃ |
| **Chamber pressure:** | 20 bar |
| **Injection Pulse width:** | 2500 µs |
| **Injection Pressure:** | 1000 bar |
| **Coolant Temperature:** | 50℃ |

$$DCN = 13.028 + \left(\frac{-5.3378}{ID}\right) + \left(\frac{300.18}{CD}\right) + \left(\frac{-1267.90}{CD^2}\right) + \left(\frac{3415.32}{CD^3}\right) \quad (1)$$

The average pressure and Apparent Heat Release Rate (AHRR) for the 15 combustion events for both IPK and Jet-A are shown in Figure 11 where it is shown that IPK is much less reactive than Jet-A as supported by Table 5.

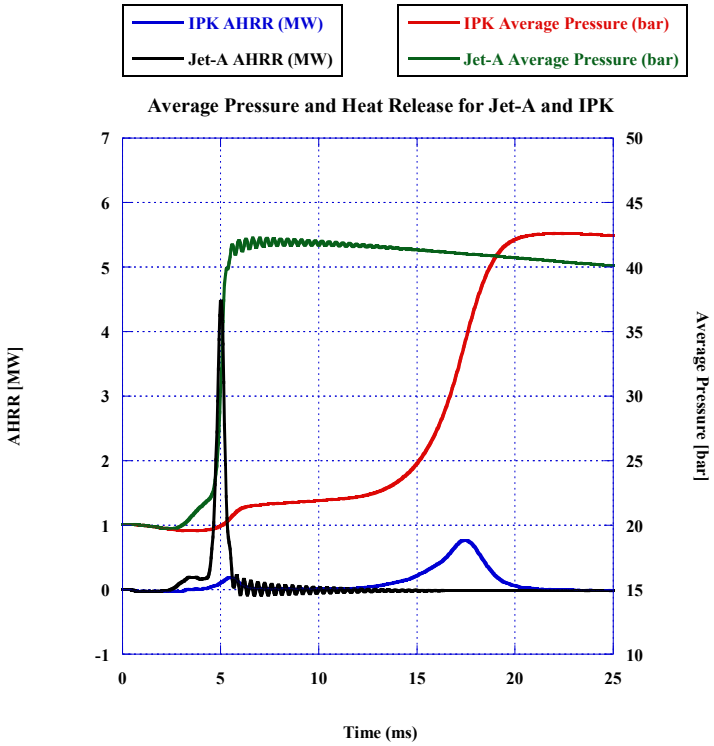


**Figure 11. Pressure and AHRR for IPK and Jet A**

As observed from Figure 11, IPK had an extended CD in comparison to Jet-A, resulting in a lower peak apparent heat release rate (AHRR) as IPK has two peaks of AHRR vs Jet-A's one peak AHRR. IPK's dual peak AHRR can be attributed to its initial low temperature heat release occurring at 5 ms followed by Jet A's high temperature heat release (HTHR) at 17 ms. IPK presents a very long Negative Temperature Coefficient Region.

**Table 5. Combustion properties for IPK and Jet A**

| Combustion Properties | IPK | Jet A |
|---|---|---|
| ID [ms] | 5.31 | 3.26 |
| CD[ms] | 17.17 | 5.01 |
| DCN | 25.88 | 47.96 |

## IV. CFD Simulation of a Single Stage Gas Turbine Engine

A computational fluid dynamic (CFD) transient combustion simulation of a single stage gas turbine engine was performed utilizing ANSYS software. A solid cavity of the internal flow sections of the engine was then created for simulation. The six injector ports were created and attached at their respective locations on the combustion chamber. A mesh was then developed inside of the modules mesh setup where a coarse mesh sizing was used to alleviate simulation time. The mesh included 1.7 million nodes and 1.02 million elements.

Setup for both boundary conditions and time step were then put into place. Two consecutive simulations with a time step of $1\times10^{-6}$ for 5000-time steps per run was performed. Both sets of reactions and material were used to simulate the combustion process. ANSYS CFX library includes a list of fuel types and from this list the Jet A fuel type was selected and imported into the reactions listing. The heat transfer, turbulence model, and combustion model were all selected and modified for Jet A fuel.

An initialization was set where the relative pressure was 0 atm and the temperature was 300°K. As this model is not static the inlet was placed directly behind the back of the compressor to avoid pressure build up issues. The inlet velocity was set to 33.70 m/s and the mass fraction was adjust so that air was the only fluid entering the combustion chamber.

A second inlet boundary condition was created and placed on all 6 injector port faces to ensure fuel was introduced at the appropriate angle and velocity. The inlet speed for the fuel was calculated based off of the compressor exit speed and RPM relationship which was found to be 101.09 m/s. The mass fraction was changed to 100% jet A fuel.

Finally, an outlet condition was placed at the back of the turbine where the exhaust exits the surrounding atmosphere. Here the static pressure was set to 0 atm to ensure the resulting gases exited the system. The geometry model of the single stage turbojet engine was modified to be compatible with CFX modeling requirements to develop an accurate flow of fluid through the model.

Simulation model produced velocity of 450 m/s at tip of impeller blades compared to 470 m/s based on manufacturer specifications.

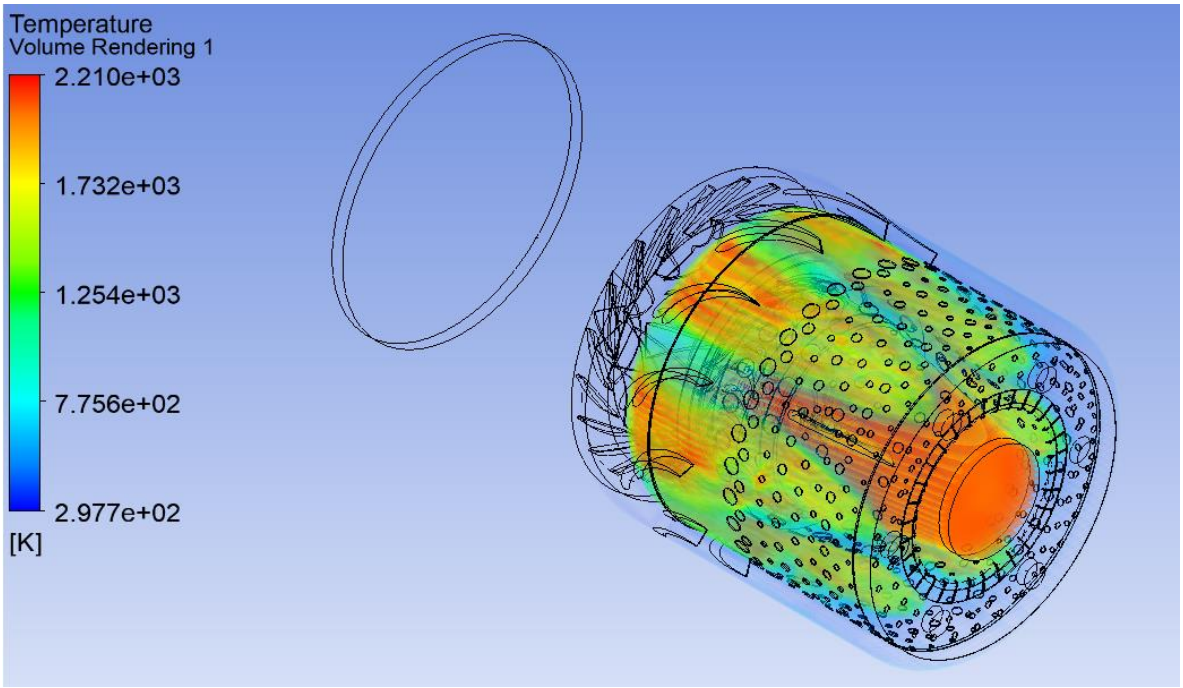


**Figure 12. Isometric View of Temperature Volume Rendering for 47,000 RPM, Jet A**

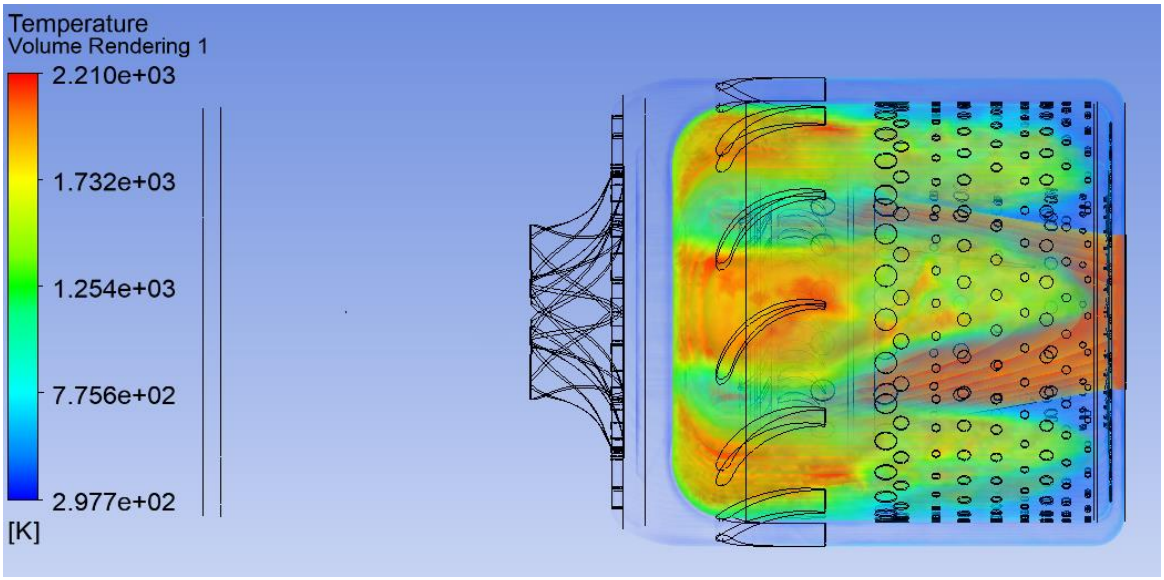


**Figure 13. Side View of Temperature Volume Rendering for 47,000 RPM, Jet A**

## V. Experimental Set Up

***Gas Turbine***

For the experiments a SR-30 experimental single stage gas turbine, pictured below was used (Turbine Techologies 2011). It is an experimental engine that was instrumented with five pressure sensors (Setra Model 209) and K-type thermocouples at each stage of the turbine. The gas turbine is also instrumented with a flow meter for the fuel flow and fuel consumption. The turbine has a button type force sensor (Futek Model LLB400) load cell sensor that can measure up to 100 lbs. The engine has a maximum operating speed of 80,000 rpm, maximum thrust of 40 lbf, pressure ratio of 3.4 to 1, and specific fuel consumption of 1.22 lbfuel/lbf-hr. The engine is designed to operate on various types of fuels such as Jet A, JP8, ULSD, biofuels, and synthetic fuels (Turbine Techologies 2011). In reference to the ANSYS simulation, the sensors on the turbine engine displayed in Figure 13 were utilized to get accurate measurements to incorporate into the model.

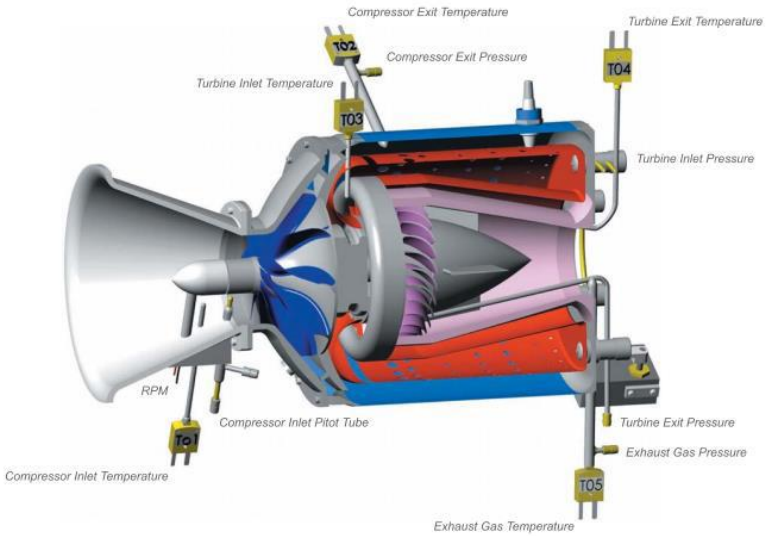


**Figure 14. Cutout view of the single stage jet engine (C. Jensen 2012)**

The DAQ board used, was a National Instruments (NI6218) analog output. The gas turbine RPM speed tested, ranged from 60,000-70,000 in the analyses discussed. To view the max operating conditions, see Table 6.

**Table 6. Maximum Operating Conditions (Turbine Technologies, 2011)**

| | |
|---|---|
| **Max RPM** | 77,000 |
| **Max Inlet Temp (°C)** | 870 |
| **Max Exhaust Temp (°C)** | 720 |
| **Max Air Pressure (kPa)** | 1,103 |
| **Max Oil Pressure (kPa)** | 70 |
| **Max Ambient Temp (°C)** | 41 |

***NVH Experimental Set Up***

To minimize sound reflective surfaces, the turbine was moved to an open test bay for experimentation. Using the pressure sensors, thermocouples, and fuel flow rate transmitters at the inlet and outlet, a National Instruments analog output model NI6218 collected pressure, temperature and flow data and displays it in a live graph while the speed (rpm) and thrust were also measured. The NI6218 transmitted and displayed the live readings to minilab software located on a designated turbine engine laptop.

Two Bruel & Kjaer (B&K) microphones were used to measure the mid to low range frequencies at the intake and exhaust nozzles as well as at the combustion chamber. A Prepolarized Free-field ½" Microphone Type 4966 was placed 1 m away from the turbine outlet (exhaust) at an angle of 45º. A Multi-field ¼" Microphone Type 4961 was placed 2 m away from the main body of the turbine, at an angle perpendicular from the main body. The specifications of the microphones are listed in Tables 7 and 8.



**Table 7. Free-field 1/2" Microphone Type 4966 Specifications**

| | |
|---|---|
| **Temperature** | 23 C |
| **Ambient Static Pressure** | 101.3 kpa |
| **Relative Humidity** | 50 % |
| **Frequency** | 251.2 Hz |
| **Polarization Voltage, external** | 0 V |
| **Combined Sensitivity** | -27.2 db re 1 V/Pa |
| **Uncertainty 95% confidence level** | 0.2 db |

**Table 8. Multi-field 1/4" Microphone Type 4961 Specifications**

| | |
|---|---|
| **Temperature** | 23 C |
| **Ambient Static Pressure** | 101.3 kpa |
| **Relative Humidity** | 50 % |
| **Frequency** | 251.2 Hz |
| **Polarization Voltage, external** | 0 V |
| **Combined Sensitivity** | -24.5 db re 1 V/Pa |
| **Uncertainty 95% confidence level** | 0.3 db |

Both microphones were mounted on tripods at a height level to that of the turbine midsection. A schematic for the orientation of the microphones can be seen in Figure 15 below.

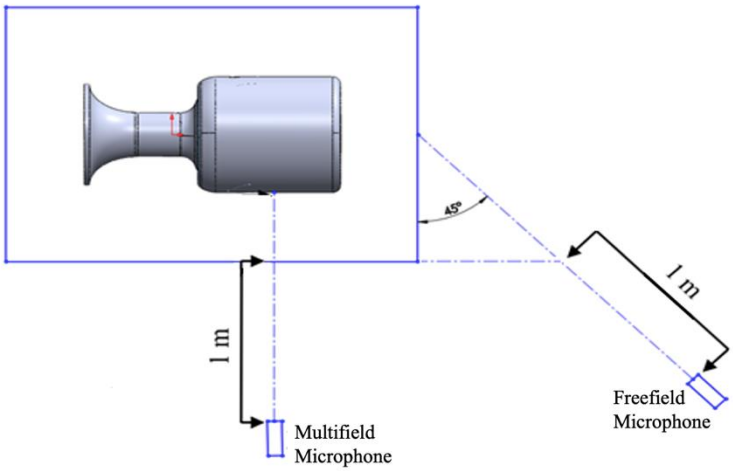


**Figure 15. Microphone Experimental Setup Schematic**

A Triaxial Deltatron B&K Accelerometer Type 4527 was used to measure movement of the turbine in three directions during the experiments. The accelerometer specifications are shown in Tables 9 and 10.

**Table 9. Triaxial Accelerometer Environmental Specifications**

| | |
|---|---|
| **Environmental Temperature Range** | -60° C to + 180°c (-76°f to +356°f) |
| **Temperature Coefficient of Sensitivity** | +0.12%/°c |
| **Temp. Transient Sensitivity** | 0.02 $ms^{-2}$/°c |
| **Magnetic Sensitivity** | 15 $ms^{-2}$/T |
| **Base Strain Sensitivity** | 0.1 $ms^{-2}$/μ€ |
| **Max. Non-destructive shock** | 50 $kms^{-2}$ peak (5100 g peak) |

**Table 10.Triaxial Accelerometer Directional Specifications**

| | **X** | **Y** | **Z** |
|---|---|---|---|
| **Reference Sensitivity** | 9.452 mv/g | 9.939 mv/g | 9.452 mvg |
| **Frequency Range (Hz) : Amplitude (±10%)** | 0.3-10k[a]<br>0.3-5.5k[b] | 0.3-10k[a]<br>0.3-5.5k[b] | 0.3-12.8k[8] |
| **Frequency Range (Hz): Phase (±5°)** | 2-10k[a]<br>2-5.5k[b] | 2-10k[a]<br>2-5.5k[b] | 2-12.8k[8] |
| **Mounted Resonance Frequency (khz)** | 30[a]<br>19[b] | 30[a]<br>17[b] | 42[a] |

As seen in Figure 16, B&K triaxial accelerometer was positioned on the turbine support plate to measure axial vibrations during combustion. Turbine axis orientations were assigned as shown in Figure 17, with the X-axis as the parallel to the turbine, Y-axis as perpendicular to the turbine, and Z-axis as the radial direction.

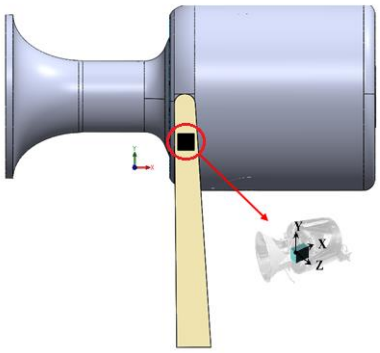

**Figure 16. Triaxial Accelerometer Experimental Placement (Kilpatrick 2019)**


**Figure 17. Turbine Axis Orientation Schematic**

***Experimental Setup Assembly and Processing***

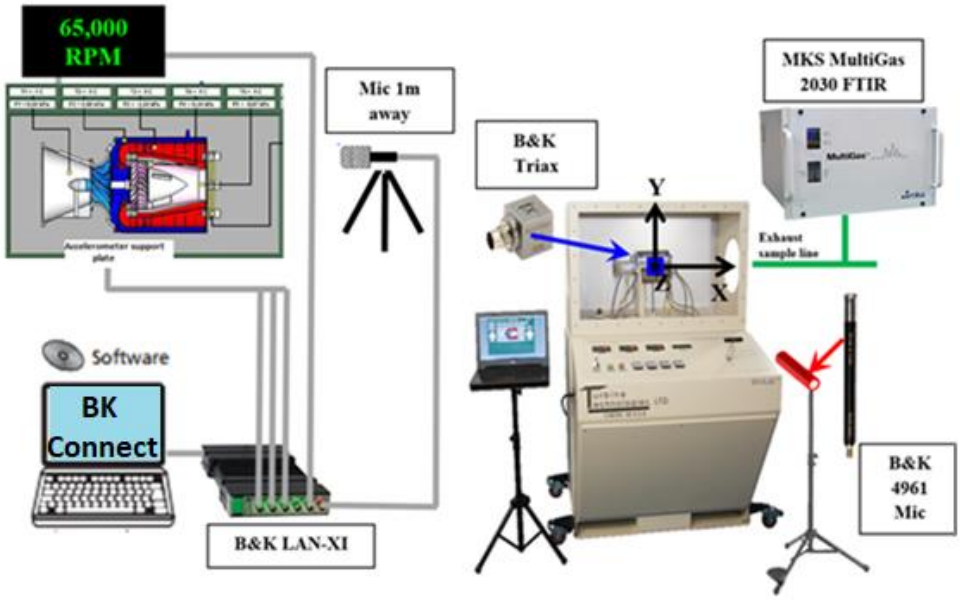


**Figure 18. Experimental Engine and Noise, Vibrations, and Emissions Instrumentation (Simons, 2016)**

For this experiment, sound pressure and acceleration measurements were taken at 65,000 RPM for Jet A and IPK and also at three different RPMs (60k, 65k and 70k) for Jet A and IPK. Gaseous emissions measurements were

also taken for Jet A and IPK comparison. BK Connect software was applied to obtain and post process the vibrations and noise data from the turbine fuel testing. Constant Percentage Bandwidth (CPB) and Fast Fourier Transformation (FFT) analysis within this software was employed to evaluate the data. The emissions data was post processed using the MKS MG2000 software within the MultiGas FTIR Spectrometer and the data produced was then analyzed.

Using the rpm sensor at the inlet of the turbine, the shaft speed was acquired. Temperature and pressure measurements were taken at the previously mentioned sensor locations on the turbine to include the areas of the compressor inlet, turbine inlet, turbine exit and exhaust. Sound pressure measurements were taken at a distance of 1m from the turbine combustion and 1m at a 45 degree angle from the turbine exhaust. The accelerometer was mounted on the turbine support plate which allowed for acceleration measurements to be taken as well. During operation these measurements were taken through the use of the measurement chain process below.

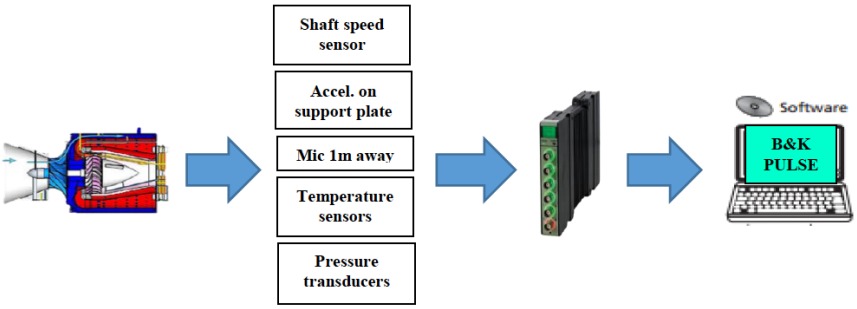


**Figure 19. Measurement chain and DAQ Processes**

For the sound level measurements, Constant Percentage Bandwidth (CPB) analysis was employed. The CPB analysis is a common way to analyze sound levels by separating the signals into the basic frequency constituents. For the acceleration (vibration) measurements, Fast Fourier Transform was employed to analyze the data. This allowed for the conversion from the time domain to a representation in the frequency domain, similar to CPB. Both the FFT and CPB analysis utilize Euler's equations for complex transformations. The bandwidth organization was based on 1/3 octave bandwidths and A weighting, as A weighting focuses on the human hearing capabilities.

The frequency range considered for the sound pressure and acceleration data was the range of 0 to 16 kHz. This was chosen in order to examine the gas turbine's behavior on a broad frequency range and identify the frequencies of key mechanical components within the turbine. All Fourier analysis was judged on the differences in decibels, specifically differences of 3 decibels or more, as humans are able to notice changes in sound at this difference level.

When discussing the frequencies of sound, the term harmonics is used to describe the distortion of a sinusoidal waveform by waveforms of different frequencies. Any waveform, whatever the complexity of its shape, can be mathematically split into individual components called the fundamental frequency and various harmonic frequencies. In relation to the research gas turbine, the fundamental frequency refers to the rotation of the main shaft. Any harmonics discussed indicate the flaws of the component responsible for the fundamental frequency signal, and an order indicates a signal from a separate component. Harmonics can inform on mechanical parts of the turbine such as worn bearings which cause a shaft to rotate imperfectly about its axis. Frequency orders are frequency correlations to different mechanical components within the turbine, to include the compressor and turbine blades. For example, the gas turbine operating at 60,000 rpm will have a fundamental frequency of 1 kHz. If the compressor consists of 12 blades, a signal will be present at 12 kHz (12×1 kHz).

## VI. Results

The following data include results from a total of four turbine runs: three runs of IPK and one run of Jet A. The results were averaged for the three turbine experiments with IPK and compared to the Jet A results.

***Gaseous Emissions***

The emissions of Jet A and IPK were measured at the exhaust and analyzed using a MKS MultiGas 2030 FTIR Spectrometer. The emissions results are displayed in the tables below. As an alternative fuel, IPK is derived from coal

using the Fischer-Tropsch process and known for having little to no aromatics, making it, in theory, a fuel less detrimental to the atmosphere as far as its emission of greenhouse gasses. These specific exhaust gases were chosen as the most crucial to monitor and mitigate in jet fuel exhaust.

**Table 11. Average Jet A and Gaseous Emissions Results at 60,000 rpm operating speed**

| Species | Jet A | IPK | % Difference between Jet A and IPK |
|---|---|---|---|
| **$H_2O$ (%)** | 4.02 | 3.06 | - 27.08% |
| **$CO_2$ (%)** | 2.93 | 2.46 | - 17.12% |
| **$NO_x$ (ppmv)** | 23.72 | 20.67 | - 13.77% |
| **CO (ppmv)** | 1195.1 | 890.91 | - 29.16% |
| **THC (ppmv)** | 2231.2 | 1481.8 | - 40.37% |

* Are shown as % of Exhaust gas sampled

**Table 12. Average Jet A and Gaseous Emissions Results at 65,000 rpm operating speed**

| Species | Jet A | IPK | % Difference between Jet A and IPK |
|---|---|---|---|
| **$H_2O$ (%)** | 4.06 | 3.19 | - 24.10% |
| **$CO_2$ (%)** | 2.95 | 2.59 | - 13.05% |
| **$NO_x$ (ppmv)** | 23.72 | 23.71 | - 0.04% |
| **CO (ppmv)** | 1062.89 | 867.47 | - 20.25% |
| **THC (ppmv)** | 1812.25 | 1338.70 | - 30.06% |

**Table 13. Average Jet A and Gaseous Emissions Results at 70,000 rpm operating speed**

| Species | Jet A | IPK | % Difference between Jet A and IPK |
|---|---|---|---|
| **$H_2O$ (%)** | 4.10 | 3.19 | - 25.05% |
| **$CO_2$ (%)** | 3.04 | 2.59 | - 16.22% |
| **$NO_x$ (ppmv)** | 27.91 | 23.71 | - 16.25% |
| **CO (ppmv)** | 968.23 | 867.47 | - 10.98% |
| **THC (ppmv)** | 1186.0 | 1342.4 | + 12.37% |

As observed in the tables, IPK was able to reduce $NO_X$, $SO_2$, $H_2O$, and $CO_2$ emissions in comparison to Jet-A in each operating speed trial. The only increase in emissions was at the 70,000 rpm operating speed with the total hydrocarbon content for IPK being 12.37% higher than that of Jet A. The reason for this occurrence is under investigation. Additionally, the emissions were analyzed in reference to the variations in operating speed of the turbine. In Figures 20-23 below, the gaseous emissions for each fuel are displayed in reference to the operating speed.

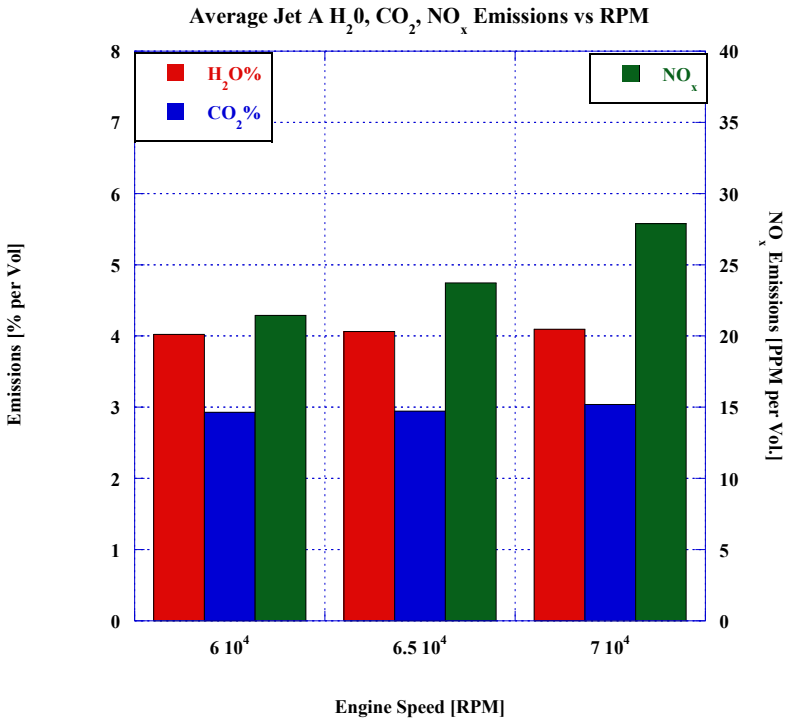


**Figure 20. Average Jet A $H_2O$, $CO_2$, and $NO_x$ Emissions vs RPM**

Figure 20 displays the Average Jet A emissions based on the operating speed. As the rpm increases, the nitrous oxide emissions substantially increase while the $H_2O$% and $CO_2$% emissions increase only marginally.

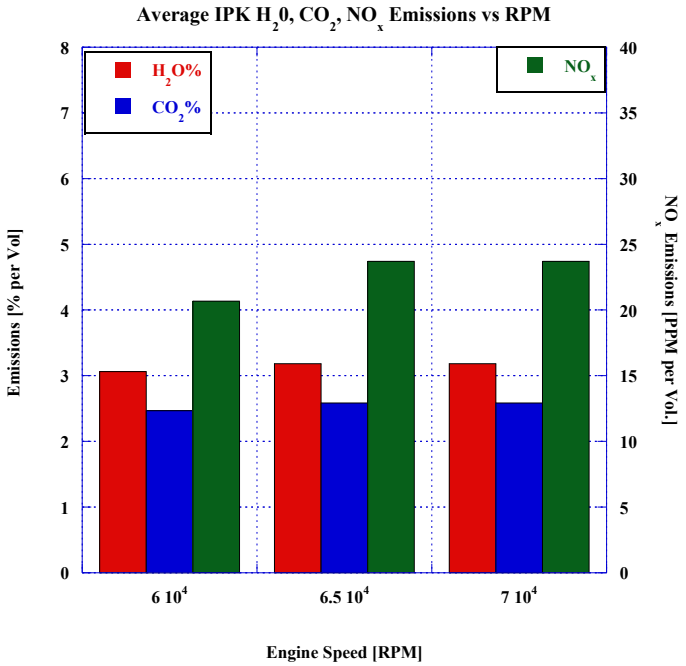


**Figure 21. Average IPK $H_2O$, $CO_2$, and $NO_x$ Emissions vs RPM**

Figure 21 displays the average IPK emissions for the three operating speeds. Again, it can be seen that the nitrous oxide emissions have a more significant increase as the rpm increases as compared to the small growth in $H_2O$% and $CO_2$% emissions.

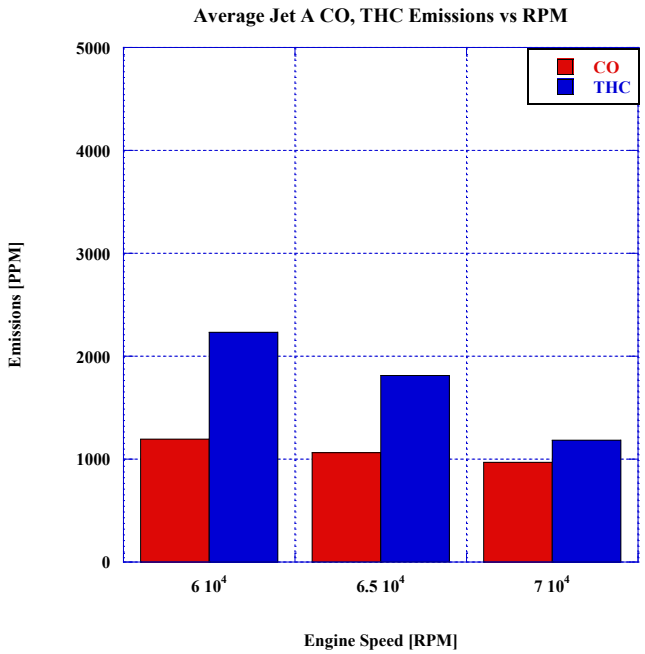


**Figure 22. Average Jet A CO, THC Emissions vs RPM**

In reference to the average Jet A CO and THC emissions, as the operating speed increased, both species of emissions decreased. THC decreased by a significant margin, while CO showed less noticeable reductions.

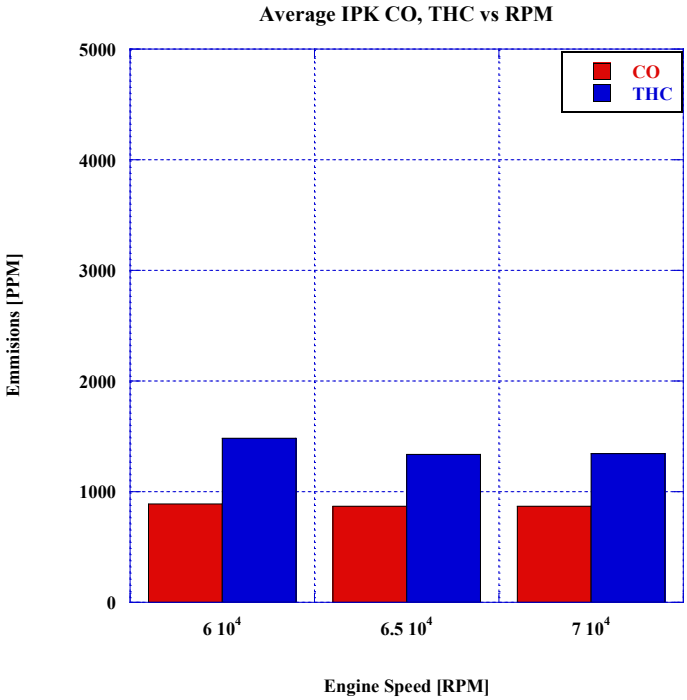


**Figure 23. Average IPK CO, THC Emissions vs RPM**

Figure 23 illustrates the average IPK CO and THC emissions at the three operating speeds. IPK showed relatively constant CO emissions across the three rpms. Meanwhile, IPK had reductions in THC emissions as the rpm of the turbine increased.

***Noise, Vibrations and Harshness Analysis***

First, the noise, vibrations, and gaseous emissions for Jet A and IPK were measured at operating speeds of 60k, 65k, and 70k RPM. The frequency range for the sound pressure data set was 8 kHz. The sound pressure measurements were processed with a CPB. While the entire range of sound pressure will be analyzed, special attention will be given to the combustor noise region, which is commonly accepted as the 200 – 500 Hz frequency region. In the following data sets, at the upper frequencies of noise (1-8kHz; higher pitches), the overall sound pressure levels reach the 90-100 dB(A)/µPa range. This 90-100 dB(A)/µPa range would be considered very loud to the human ear. Figure 24 below displays the unweighted one-third octave band analysis of the sound pressure levels of IPK and Jet A for 60,000 rpm operating speed.

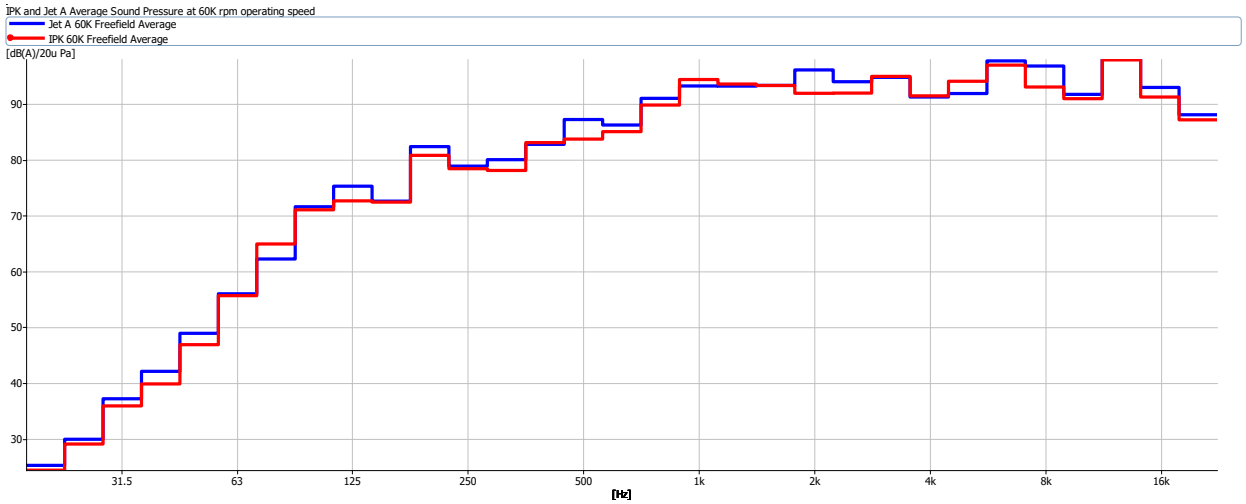


**Figure 24. IPK and Jet A Sound Pressure Summary at 60,000 rpm operating speed**

At 60,000 rpm operating speed, there is certainly a general trend to the data, with the sound pressure measurement for Jet A and IPK closely resembling each other. In the combustor region (200-500 Hz), Jet A shows higher amplitudes of sound pressure in comparison to IPK. Figure 25 below displays the unweighted one-third octave band analysis of the sound pressure levels of IPK and Jet A for 65,000 rpm operating speed.

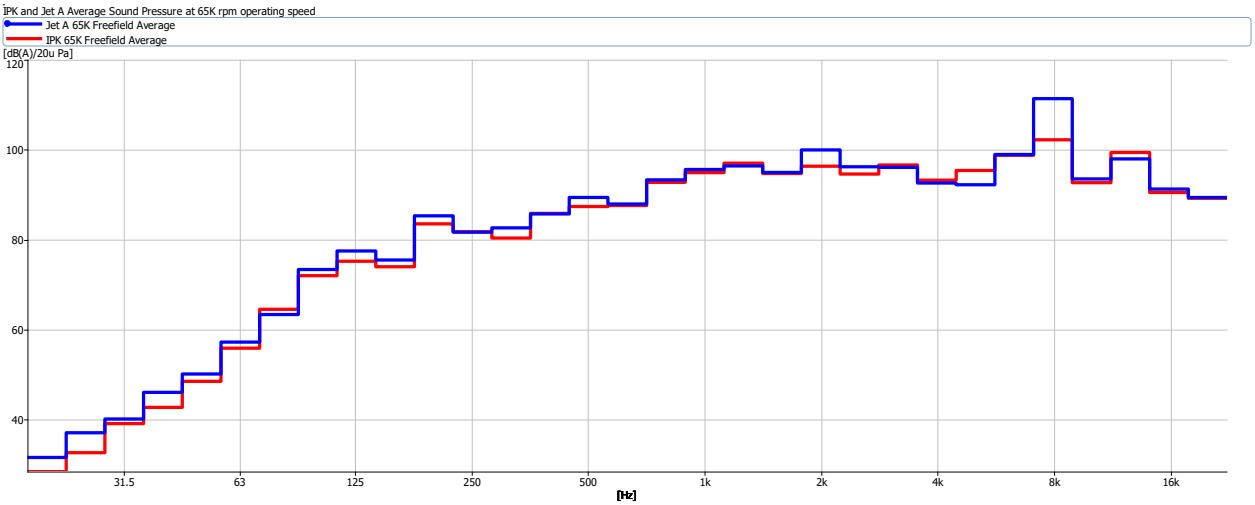


**Figure 25. IPK and Jet A Sound Pressure Summary at 65,000 rpm operating speed**

At 65,000 rpm operating speed, the IPK and Jet A sound pressure curves continue to follow the same trends. There are clear peaks in the Jet A sound pressure at the 2 kHz and 8 kHz frequency locations. In the combustor frequency range, Jet A again shows slightly higher sound pressure levels than IPK. Figure 26 below displays the unweighted one-third octave band analysis of the sound pressure levels of IPK and Jet A for 70,000 rpm operating speed.

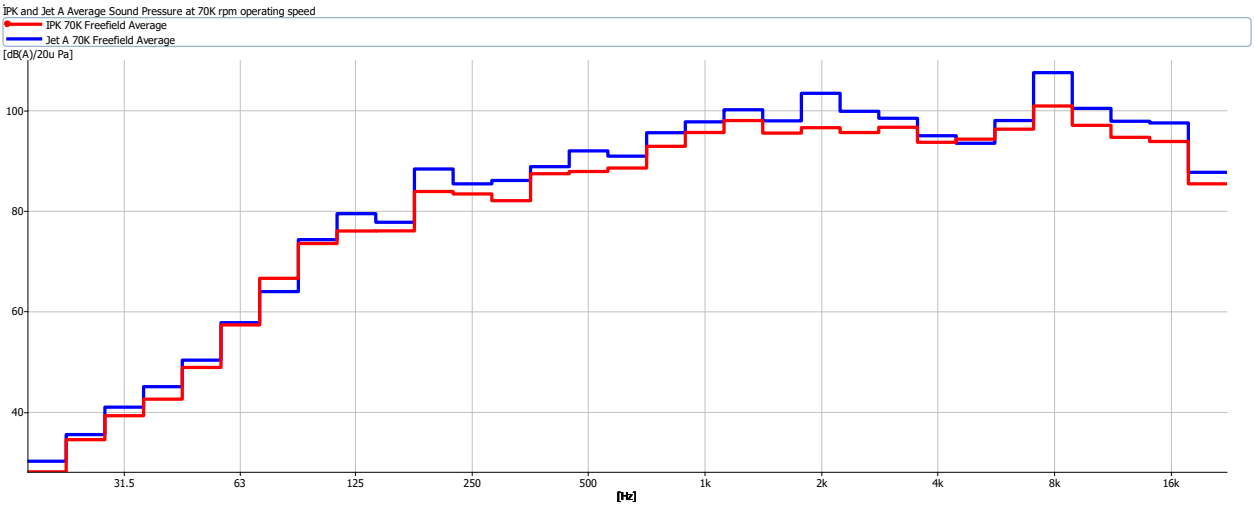


**Figure 26. IPK and Jet A Sound Pressure Summary at 70,000 rpm operating speed**

At 70,000 rpm operating speed, Jet A shows a significantly increased sound pressure profile across the entire frequency range (0-8kHz). Jet A has higher amplitudes of sound pressure in the combustor region (200-500 Hz range) as compared to IPK. Across the three speeds, IPK has a quieter sound profile than Jet A. At 70,000 rpm speed, Jet A shows the most substantial difference in sound pressure levels compared to IPK.

In addition to sound pressure measurements, acceleration data was also obtained at three different speeds (60,000 rpm, 65,000 rpm, and 70,000 rpm) for the two fuels. The triaxial vibration measurements for each trial were first processed using FFT, then the vector sum of the three directional accelerations was obtained. The vector sum of acceleration from each trial was averaged to display an overall acceleration measurement. The overall spectrum for each set of vibration measurements clearly indicates orders that were excited the most. The vibration amplitude is presented in dB with 1 $\mu m/s^2$ reference. The locations of primary concern for the vibration data set are as follows: around 1 kHz, which correlated to shaft rotation (60,000 rpm = 1,000 Hz; 65,000 rpm = 1,083 Hz; 70,000 rpm = 1,167 Hz), the third order at 3kHz, matching up to the three turbine exit blades (three blades, 3 × 1,083 Hz = 3,249 Hz), and the twelfth order at 13 kHz, corresponding to the compressor blades (twelve blades, 12 × 1,083 Hz = 12,996 Hz). For each RPM, the corresponding operating frequency and additional frequencies for consideration are shown in the table below.

**Table 14. Mechanical Properties of the Aero-Gas Turbine and Corresponding Frequencies**

| RPM | 60,000 | 65,000 | 70,000 |
|---|---|---|---|
| **Operating Frequency – Shaft Rotation** | 1,000 Hz | 1,083 Hz | 1,167 Hz |
| **3 Fins** | 3,000 Hz | 3,250 Hz | 3,501Hz |
| **12 Compressor Blades** | 12,000 Hz | 13,000 Hz | 14,004 Hz |

Figure 27 below describes the vibrations of IPK and Jet A in the turbine at 60,000 rpm operating speed.

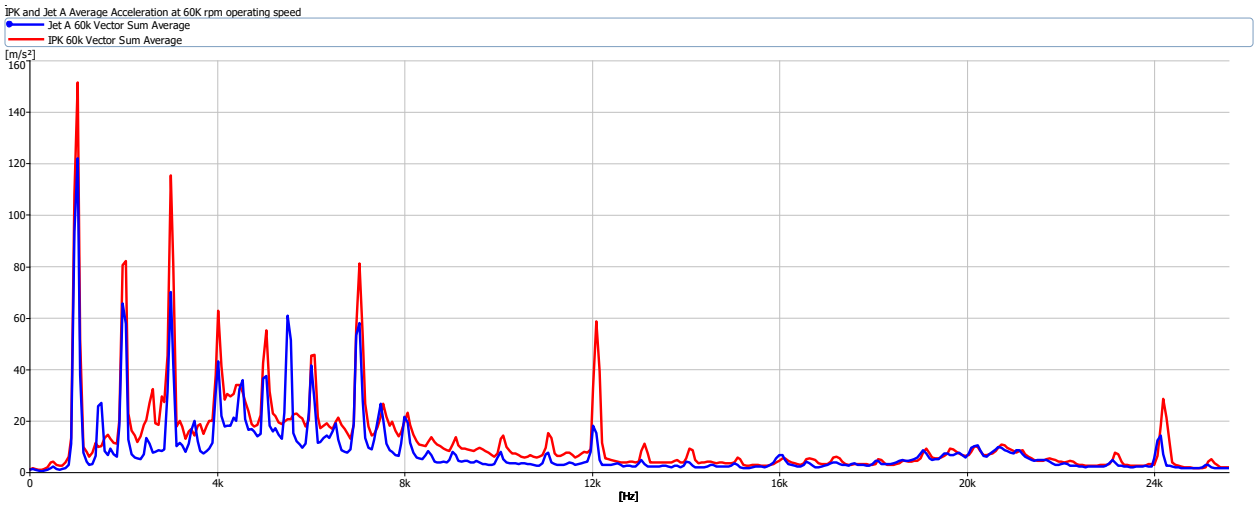


**Figure 27. IPK and Jet A Acceleration Profiles at 60,000 rpm operating speed**

Across the frequencies analyzed at 60,000 rpm operating speed, Jet A showed lower vibrational amplitudes in comparison to IPK suggesting a smoother combustion. At the 1 kHz frequency location corresponding to the shaft rotation, IPK showed an acceleration of 152 $\frac{m}{s^2}$, while Jet A displayed only 121 $\frac{m}{s^2}$. At the 3 kHz frequency correlating to the three turbine exit fins, IPK peaked at 117 $\frac{m}{s^2}$ and Jet A reached a height of only 70 $\frac{m}{s^2}$. Also, at the 12 kHz frequency, IPK reached a value of 59.5 $\frac{m}{s^2}$, whereas Jet A only peaked at 19.5 $\frac{m}{s^2}$. At the upper frequencies of vibrations (12 kHz – 24 kHz), the two fuels follow the same trend very closely, with a final peak occurring for both fuels at 24 kHz. At this final peak, IPK again displays higher amplitudes of vibrations. There are a few irregularities in the vibration curves, namely at the 1.5 kHz and 5.5 kHz frequencies. The causes of these irregularities are unknown at this time. Figure 28 below describes the vibrations of IPK and Jet A in the turbine at 65,000 rpm operating speed.

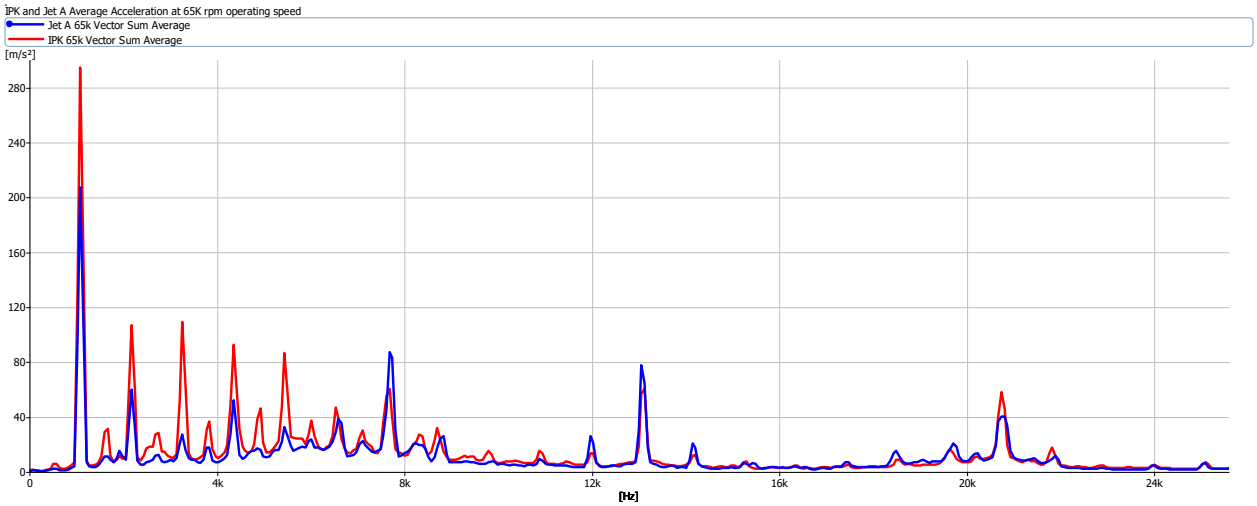


**Figure 28. IPK and Jet A Acceleration Profiles at 65,000 rpm operating speed**

Across the lower frequencies (0-8kHz) at 65,000 rpm operating speed, it is obvious that IPK has a higher general amplitude of acceleration than Jet A. There are a few cases of Jet A showing higher vibration levels at peak locations such as just before the 8kHz region and around the 13 kHz region, but other than those, IPK shows more vibrational disturbance overall. At the 1 kHz frequency location correlating to the shaft rotation, IPK reaches a maximum acceleration of 253.526 $\frac{m}{s^2}$, with Jet A showing significantly lower acceleration of 176.356 $\frac{m}{s^2}$. Around the 3.2kHz frequency location corresponding to the three turbine exit fins, IPK reads 96.84 $\frac{m}{s^2}$ acceleration with Jet A only displaying 22.58 $\frac{m}{s^2}$ acceleration. Aside from the specific frequency locations of interest in the 0-8kHz frequency range,

IPK also has greater levels of acceleration in each of the normal short vibrational peaks that are seen between 1 kHz and 8 kHz.

In the 8-24 kHz frequency range of the 65,000 rpm operating speed, the fuels follow the same general trend. In this range, it can be seen that while the vibration measurements are much less disparate than in the lower frequency range, Jet A actually shows higher acceleration than IPK at most of the peaks. Around the 8 kHz region, Jet A reaches an extreme value of 83 $\frac{m}{s^2}$ with IPK showing a reading of 55 $\frac{m}{s^2}$. The spike in the 8 kHz region could mean significant mechanical movement in the ball bearings of the turbine in the radial direction. At the 13 kHz region (12 compressor blades), Jet A again expresses a higher acceleration of 73 $\frac{m}{s^2}$ while IPK displays 47 $\frac{m}{s^2}$ acceleration. Reasoning for why Jet A has higher vibrational patterns than IPK at higher frequencies is unknown at this time. Figure 29 below describes the vibrations of IPK and Jet A in the turbine at 70,000 rpm operating speed.

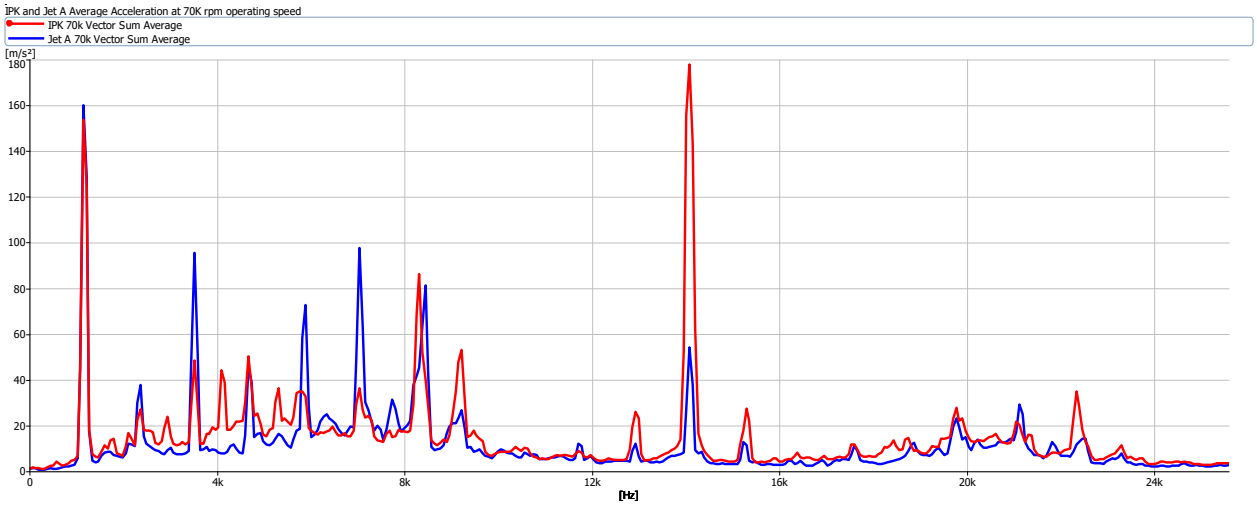


**Figure 29. IPK and Jet A Acceleration Profiles at 70,000 rpm operating speed**

At the 70,000 rpm operating speed, there are various large irregularities when comparing the IPK and Jet A fuel vibrational patterns. At the 1.167 kHz frequency related to the shaft rotation, there is a uniform spike across both fuels, this time with Jet A reaching a slightly higher amplitude than IPK. At the 3.5 kHz frequency corresponding to the three turbine exit fins, Jet A shows a significantly higher vibrational amplitude as it reaches a value of 97 $\frac{m}{s^2}$, compared to IPK's peak of 50 $\frac{m}{s^2}$. In between 4 kHz and 10 kHz, there are numerous vibrational disturbances for both fuels. Between the two fuels, Jet A shows higher amplitudes of vibrational disturbances than IPK. The reasons for these disturbances are unknown and are not paralleled at any other speeds. At the 14 kHz frequency that corresponds to the 12 compressor blades, IPK displayed an extreme value of 179 $\frac{m}{s^2}$, with a very large gap between the Jet A peak value of 56 $\frac{m}{s^2}$. Beyond the 14 kHz frequency, there are smaller irregularities between the two fuel's vibrational signatures.

Between the three operating speeds, IPK had more instances of higher amplitudes of vibrations as compared to Jet A. The higher vibrations in the IPK profile as compared to Jet A is most likely due to the low temperature heat release that IPK displays during combustion. IPK has a higher ignition delay and combustion delay which produces a more unstable combustion reaction. Additionally, this causes IPK to have a greater endothermic and exothermic reactions in comparison to Jet A and results in higher amplitudes of combustion vibrations in the shaft and three turbine exit fins when IPK is employed. Additionally, as the turbine operates at faster speeds, vibrational instabilities are shown in the compressor blades frequency locations.

## VII. Conclusions

A comprehensive study of fuel properties, experimental combustion, gaseous emissions, and noise and vibrations of IPK and Jet A was performed in a drone jet engine. Additionally, simulated combustion was modeled via CFD. The IPK density and viscosity and LHV were lower than that of Jet A with impact on spray, combustion and emissions. The Thermo Gravity and Differential Thermo Analysis showed that IPK vaporized faster than Jet A. The

Mie scattering analysis of their sprays showed that SMD of IPK is smaller suggesting that it is capable of producing finer atomization and earlier mixtures than Jet. A. The Constant Volume Combustion Chamber investigations found a very low DCN of IPK compared to Jet A while producing an early LTHR and a reduced HTHR of low values compared to HTHR of Jet A for the ASTM parameters. The IPK exhibited also a very long Negative Temperature Coefficient Region. These combined factors impacted the fuel burn of IPK within the turbine, suggesting that could lead to combustion instabilities which have been reflected by slightly higher vibrations observed with IPK.

In terms of noise and vibrations in the single stage jet engine, while it seems that the signature of the two fuels are similar, Jet A had higher sound pressure levels across the three speeds and range of frequencies measured. Additionally, IPK was most substantially quieter than Jet A at the 70,000 rpm operating speed. IPK produced smaller amounts of gaseous emissions than Jet A in every species analyzed. The research will continue to bring more information about the neat IPK characteristics in a jet engine.

## VIII. Further Research

Experimentation of Jet A is still required in order to compare the NVH and gaseous emissions profile to that of IPK. A deeper analysis of the IPK vibrational profile is also necessary. Further refinement of simulation mesh and model is necessary to reduce error in results. Transient simulation, sliding mesh, and addition of combustion analysis will also be implemented.

## IX. Acknowledgments

This research was supported by DoD-NSF Assure REU Site Award: 1950207 and the experimental fuel was provided by the Air Force Research Laboratory.

We acknowledge also the technical support of the following: Perry Kuznar, Tom Kutrieb and Kevin Carlson from Turbine Technologies LTD, Charles McGuffy and Janusz Waszkielewicz from PAC, Tanner Smith, Tony Frazer, Ryan Salmon, and Alfonso Moreira from Brüel and Kjær, Joseph Wolfgang from Malvern Lasers, and Timothy Martin from MKS Instruments Inc.

## X. References


AJ, Hede. 2017. "Using Mindfulness to Reduce the Health Effects of Community Reaction to Aircraft Noise." *Noise Health* 165-173.

2005. *Aviation & Emissions A Primer.* Policy, Federal Aviation Administration Office of Environment and Energy.

Badami, M., P. Nuccio, D. Pastrone, and A. Signoretto. 2014. "Performance of a small-scale turbojet engine fed with traditional and alternative fuels." *Energy Conversion and Management* 219-228.

Balachandar Gopalakrishnan, Namita Khanna, Debabrata Das. 2019. "Chapter 4: Dark-Fermentative Biohydrogen Production." In *Biohydrogen*, 79-122. Elsevier.

Bengisu, Turgay M. 2001. *Vibration Order Shift and its Computation.* Michigan: General Motors Corporation.

Bruel & Kjaer. 1982. "Measuring Vibration." Naerum, Denmark: Bruel & Kjaer, September.

—. 1984. "Meauring Sound." Naerum, Denmark: Bruel and Kjaer, September.

Bruel & Kjear. n.d. "Bruel & Kjaer." *bksv.* Accessed November 28, 2017. https://www.bksv.com/media/doc/bn1251.pdf.

C. Jensen, H. Lebreton, S. Nielsen, K. Rasmussen. 2012. *Modeling and Validation of the SR-30 Turbojet Engine.* Aalborg University.

C. Zhang, X. Hui, Y. Lin, C. Sung. 2016. "Recent Development in Studies of Alternative Jet Fuel Combustion: Progress, Challenges, and Opportunities." *Renewables and Sustainable Energy Reviews, 54* 120-138.

Chi Zhang, Xin Hui, Yuzhen Lin, Chih-Jen Sung. 2014. ""Recent development in studies of alternative jet fuel combustion: Progress, challenges, and opportunities."." *Renewable and Sustainable Energy Reviews 126* (Renewable and Sustainable Energy Reviews 126).

Dowling, Ann P., and Yasser Mahmoudi. 2014. "Combustion Noise." *Proceedings of the Combustion Institute.* Cambridge, United Kingdom: Elsevier. 65-100.

Elliot, Dave. 2015. "Aircraft Engine Noise Research and Testing at the NASA Glenn Research Center." Toledo, Ohio: NASA Glenn Research Center, November 6.

EPA. 2016. *Climate Change Indicators: Oceans.* August 2. Accessed March 2020. https://www.epa.gov/climate-indicators/oceans.

Fleming, Susan. 2009. "Aviation and Climate Change: Aircraft Emissions Expected to Grow, but Technological and Operational Improvements and Government Policies Can Help Control Emissions." *Congressional Committee.* Washington D.C.: United States Accountability Office.

Fooladgar, Ehsan, Pal Toth, and Christophe Duwig. 2019. "Characterization of flameless combustion in a model gas turbine combustor using a novel post-processing tool." *Combustion and Flame* (Elsevier) 204: 356-367. Accessed 7 28, 2020. doi:https://doi.org/10.1016/j.combustflame.2019.03.015.

Frazer, Tony. 2015. "Moving-Source Beamforming." Bruel & Kjaer.

Ghosh P., Jaffe S. B. 2006. "Detailed Composition-Based Model for Predicting the Cetane Number of Diesel Fuels." *Industrial & Engineering Chemistry Research* 346-351.

Giampaolo, Tony. 2014. *Gas Turbine Handbook: Principles and Practice.* Lilburn, GA: The Fairmont Press, Inc.

Gicquel, L.Y.M., G. Staffelbach, and T. Poinsot. 2012. "Large eddy simulation of gaseous flames in gas turbine combustion chambers." *Progress in Energy and Combustion Science* (Elsevier) 38: 782-817. Accessed 7 28, 2020. doi:http://dx.doi.org/10.1016/j.pecs.2012.04.004.

Ho, P. Y., and R. N. Tedrick. 1972. "Combustion Noise Prediction Techniquesfor Small Gas Turbine Engines." *Inter-noise Proceedings* 507-512.

Horvath, Csaba, Edmane Envia, and Gary G. Podboy. 2013. "Limitations of Phased Array Beamforming in Open Rotor Noise Source Imaging." *19th Aeroacoustics Conference.* Berlin, Germany: American Institute of Aeronautica and Astronautica and Confederation Of European Aerospace Societies. 20.

Howe, M.S. 2010. "Indirect Combustion Noise." *Journal of Fluid Mechanics* 267-288.

Hultgren, Lennart S., and Rene O. Arechiga. 2016. *Full-Scale Turbofan Engine Noise-Source Separation Using a Four-Signal Method.* Cleveland, Ohio, November 1.

International, ASTM. 2015. "Standard Specification for Aviation Turbine Fuel Containing Synthesized Hydor Carbons." West Conshohovken, PA: ASTM International.

International, ASTM. 2016. *Standard Test Method for Determination of Derived Cetane Number (DCN) of Diesel Fuel Oil- Ignition Delay and Combustion Delay Using a Constant Volume Combustion Chamber Method.* Standard, West Conshohocken, PA: ASTM.

J. Yanowitz, M.A. Ratcliff, R.L. McCormick, J.D. Taylor, M.J. Murphy. 2017. *Compendium of Experimental Cetane Numbers.* Technical, National Renewable Energy Laboratory.

J.I. Hileman, R. W. Stratton. 2017. "Alternative Jet Fuel Feasibility." *Transport Policy* 52-62.

Julia Heimberger, Martin Muinos. n.d. "Synthetic Aviation Fuels." Statesboro: Georgia Southern University.

Khandelwal, Bhupendra, Swapneel Roy, Charles Lord, and Blakey. 2014. "Comparison of Vibrations and Emissions of Conventional Jet Fuel with Stresses 100% SPK and Fully Formulated Synthetic Jet Fuel." *Aerospace* 52-66.

Kiameh, P. 2002. *Power Generation Handbook: Selection, Applications, Operation, Maintenance.* McGraw Hill Professional.

Kilpatrick, Margaret. 2019. "The Investigation of Noise, Vibrations, and Emissions of Aero-Gas Turbine Combustion wiht Synthetic Kerosens." *Honors Undergraduate Thesis.* Statesboro: Georgia Southern University.

Kjaer, Bruel and. 2016. "Product Data: PULSE Array Acoustics, Refined Beamforming Calculations BZ-5639." *Bruel and Kjaer Sound and Vibration.* September. Accessed November 15, 2017. www.bksv.com.

Kjear, Bruel and. 2004. "Technical Review: Beamforming." *Bruel and Kjear Sound and Vibrations* . November 1. Accessed November 15, 2017. www.bksv.com.

Lefebvre, Arthur H., and Dilip R. Ballal. 2010. *Gas Turbine Combustion Alternative Fuels and Emissions.* Boca Raton, FL: CRC Press.

Liu, Yu, Ann P. Dowling, Nedunchezhian Swaminathan, and Thomas D. Dunstan. 2012. "Spatial Correlation of Heat Release Rate and Sound Emission from Turbulent Premixed Flames." *Combustion and Flame* 2430-2440.

M. Gorji-Bandpy, M. Asimi. 2012. "Airframe Noise Sources Reduction Technologies in Aircraft." *Noise & Vibration Worldwide* 29-36.

Mahan, J. R. 1983. "Experimental Study ofnthe Thermal-Acoustic Efficienccy in a Long Turbulent Diffusion-Flame Burner." *National Aeronautics and Space Administration Technical Papers Server.* February 1. Accessed September 17, 2017. https://ntrs.nasa.gov/search.jsp?R=19830011553#?

Mofid Gorji-Bandpy, Mohammadreza Azimi. 2012. "Airframe Noise Sources and Reduction Technologies in Aircraft." *Noise and Vibration Worldwide* 29-32.

Mohamad P. Zakaria, Chui-Wei Bong, Vahab Vaezzadeh. 2018. "Chapter 16 - Fingerprinting of Petroleum Hydrocarbons in Malaysia Using Environmental Forensic Techniques: A 20-Year Field Data Review." *Oil Spill Environmental Forensics Case Studies* 345-372.

N. A. O. Engineering. 2010. *Technology for a Quieter America.* Washington D.C.: The National Academies Press.

2018. "Noise Control Suppression." *Purdue School of Aeronautics and Astronautics.* Accessed March 10, 2020. https://engineering.purdue.edu/~propulsi/propulsion/jets/basics/noise.html.

Occupational Safety and Health Administration. 2008. *United States Department of Labor.* December 12. Accessed November 3, 2017. https://www.osha.gov.

R., Cataluna R. and d. Silva. 2012. "Effect of Cetane Number on Specific Fuel Consumption and Particulate Matter and Unburned Hydrocarbon Emissions from Diesel Engines." *Journal of Combustion.*

Richard Striebich, Linda Shafer, Matthew J. DeWitt, and Zachary West. 2008. *DEPENDENCE OF FUEL PROPERTIES DURING BLENDING OF ISO-PARAFFINIC KEROSENE AND PETROLEUM-DERIVED JET FUEL* . Government Interim, WRIGHT-PATTERSON AIR FORCE BASE, OH: University of Dayton Research Institute.

Robert J. Santoro, Thomas A Litzinger. 2007. *Generation of Comprehensive Surrogate Models and Validation Databases for Simulating Large Molecular Weight Hydrocarbon Fuels.* Princeton, NJ, September 17.

Romera, M.B. 2018. *Regime Interaction and Climate Change: The Cae of International Aviation and Maritime Transport.* London: Routledge: Taylor and Francis Group.

Rotaru, Constantin. 2017. "Flow field analysis of turbojet combustion chamber." *9th International Scientific Conference on Aeronautics, Automotive and Railway Engineering and Technologies.* Brasov: EDP Sciences. 01008. Accessed 7 28, 2020. doi:https://doi.org/10.1051/matecconf/201713301008.

Ryder, R., R. C. Hendricks, M. L. Huber, and D. T. Shouse. 2010. "Computational Analysis of Dynamic SPK(S8)-JP8 Fueled Combustor-Sector Performance." *Proceedings of the 13th International Symposium on Transport Phenomena and Dynamics of Rotation Machinery (ISROMC13'10).* Ivoryton. Accessed 11 15, 2019.

Sadeghbeigi, Reza. 2012. "Chapter 3 - FCC Feed Characterization." In *Fluid Catalytic Cracking Handbook (Third Edition)*, 51-86. Butterworth-Heinemann.

Shakeel, Mohammad Raghib, Yinka S. Sanusi, and Esmail M. A. Mokheimer. 2017. "Numerical Modeling of Oxy-Fuel Combustion in a Model Gas Turbine Combustor: Effect of Combustion Chemistry and Radiation Model." *9th International Conference on Applied Energy.* Cardiff: Elsevier . 1647-1652. Accessed 7 4, 2020. doi:https://doi.org/10.1016/j.egypro.2017.12.544.

Shivashankara, Belur N., and Robert W. Crouch. 1977. "Noise Characteristics of a Can-Type Combustor." *Journal of Aircraft* 751-756.

Simons, Erica. 2016. "Investigations of the Combustion Sound and Vibration Characteristics of an Aero-derivative Gas Turbine." *Electronic Thesis and Dissertaions.* https://digitalcommons.georgiasouthern.edu/etd/1516.

Soloiu, Valentin, Aliyah Knowles, Emerald Simons, and Martin Muinos. 2016. "Aircraft Turbine Sound and Vibrations Signatures for a Synthetic Kerosene Fuel." *Proceedings of the ASME 2016 International Mechanical Engineering Congress and Exposition.* Phoenix, AZ: American Society of Mechanical Engineers.

Soloiu, Valentin, Aliyah Knowles, Jose Moncada, Emerald Simons, Martin Muinos, and Huong Kim Ngo. 2017. "Small Aircraft Turbine Noise from Combsution of Synthetic Kerosene Fuels." *Proceedings of the ASME 2017 Turbomachinery Conference and Exposition.* Charlotte, NC: American Society of Mechanical Engineers.

Stein, Theo. 2020. *Aviation is responsible for 3.5 percent of climate change, study finds.* September 3. https://research.noaa.gov/article/ArtMID/587/ArticleID/2667/Aviation-is-responsible-for-35-percent-of-climate-change-study-finds.

Strahle, W. C. 1972. "Some Results in Combustion Generated Noise." *Journal of Sound and Vibration* 113-125.

Strahle, Warren C., and B. N. Shivashankara. 1975. "A Rational Correlation of Combustion Noise Results From Open Turbulent Premixed Flames." *Combustion Noise* 1379-1385.

Swift, Hales. 2010. "A Review of Literature Related to Potential Health Effects of Aircraft Noise." *Cooperative Agreement.* Lafayette, Indiana: Federal Aviation Administration Office of Environment.

Sylvester Abanteriba, Ulas Yildirim, Renee Webster, David Evans and Paul Rawson. 2016. "Derived Cetane Number, Distillation and Ignition Delay Properties of Diesel and Jet Fuels Containing Blended Synthetic Paraffinic Mixtures." *SAE International Journal of Fuels and Lubricants* 703-711.

Tara J Fortin, Arno Laesecke. 2015. "Viscosity Measurements of Avition Turbine Fuels." *Energy and Fuels 12.*

Turbine Techologies. 2011. "MiniLab Operator's Manual." Chetek, WI: Service Publications.

Tyliszczak, Artur, Andrzej Boguslawski, and Dariusz Nowak. 2016. "Numerical simulation of combustion process in a gas turbine with a single and multi-point fuel injection system." *Applied Energy* (Elsevier) 174: 153-165. Accessed 7 28, 2020. doi:http://dx.doi.org/10.1016/j.apenergy.2016.04.106.

Wawrzak, Karol, Andrzej Boguslawski, Artur Tyliszczak, and Michal Saczek. 2019. "LES study of global instability in annular jets." *International Journal of Heat and Fluid Flow* (Elsevier) 79: 108460. Accessed 7 7, 2020. doi:https://doi.org/10.1016/j.ijheatfluidflow.2019.108460.

Yi Yang, André L. Boehman, Robert J. Santoro. 2007. "A study of jet fuel sooting tendency using the trheshold sooting index model." In *Combustion and Flame*, 191-205. Elsevier.

Zettervall, N., N.A. Worth, M. Mazur, J.R. Dawson, and C. Fureby. 2019. "Large eddy simulation of CH4-air and C2H4-air combustion in a model annular gas turbine combustor." *Proceedings of the Combustion Institute* (Elsevier) 37: 5223-5231. Accessed 7 28, 2020. doi:https://doi.org/10.1016/j.proci.2018.06.021.

Zhou, Li, Zeng-wen Liu, and Zhan-xue Wang. 2015. "Numerical study of influence of biofuels on the combustion characteristics and performance of aircraft engine system." *Applied Thermal Engineering* 399-407.